AQPs have been identified in DCs, including AQP3, 5, 7, and 9 in human DCs generated from peripheral blood mononuclear cells (PBMCs) (20, 21) and AQP5 in mice bone marrow monocyte-derived DCs (BMDCs) (22). Moreover, our preliminary experiment found that AQP3 and 7 were expressed in mice skin DCs. The study using AQP inhibitors in human PBMC-derived DCs suggested that AQPs might play a role in the process of antigen uptake *via* fluid phase macropinocytosis (20). The experiment on AQP5-knockout mice showed the decrease in endocytotic ability in AQP5-deficient BMDCs (22). These previous studies suggested the involvement of AQPs in antigen uptake in monocyte-derived DCs; however, a functional characterization of specific AQPs in cutaneous DCs has not yet been elucidated.

This study focuses on the role of AQP7 in skin DCs because another study from our laboratory found that AQP3 expression had little effect on DC function (unpublished results). We tested the hypothesis that AQP7 is involved in macropinocytosis and/or phagocytosis, specifically antigen uptake, which is required for antigen-induced cutaneous immune responses. For these studies, we utilized AQP7-deficient mice (23) and isolated LCs and dDCs from mouse skin. We found that AQP7 is functionally expressed in mouse skin DCs and is involved in antigen uptake, cell migration, and the subsequent initiation of an immune reaction. Our data suggest that AQP7 may play an important role in allergy induction and immune surveillance in the skin and in other tissues in which DCs are localized.

MATERIALS AND METHODS

Mice

AQP7-knockout ($AQP7^{-/-}$) mice (C57BL/6 genetic background) were generated by targeted gene disruption (23). All animal experiments were approved by the Committee on Animal Research of Kyoto University.

Cutaneous cell preparation and cultures

Skin was incubated with dispase (5 U/ml; Life Technologies, Grand Island, NY, USA) for 1 h at 37°C to separate the dermis and epidermis. The epidermis was incubated in enzyme-free cell dissociation buffer (20 min, 37°C; Millipore, Bedford, MA, USA) to isolate single cells. The dermis was incubated in collagenase type II (500 U/ml; Worthington Biochemicals, Lakewood, NJ, USA) for 1 h at 37°C. All solutions were dissolved in complete RPMI (cRPMI) containing 10% heat-inactivated fetal calf serum (Invitrogen, Carlsbad, CA, USA), 50 μM 2-mercaptoethanol (Sigma, St. Louis, MO, USA), 2 mM L-glutamine, 25 mM HEPES, 100 μM nonessential amino acids, and 10 μM sodium pyruvate (Invitrogen).

Quantitative RT-PCR

$CD11c^+$ cells were isolated from epidermal or dermal cell suspensions using CD11c microbeads with the AutoMACS system (Miltenyi Biotech, Gladbach, Germany) per the manufacturer's protocol. Total RNA was extracted using TRIzol (Invitrogen). The cDNA was reverse transcribed from total RNA samples using the Prime Script RT reagent kit (Takara Bio, Otsu, Japan). Quantitative RT-PCR was performed using SYBR Green I (Takara Bio) and the Light Cycler real-time PCR apparatus (Roche, Mannheim, Germany).

Immunofluorescence

The isolated LCs were cultured on polylysine-coated coverslips and were fixed with 4% formalin in PBS. Cells were permeabilized with 0.1% saponin and stained with anti-AQP7 (AB15568; Millipore) and a FITC-conjugated anti-rabbit IgG secondary antibody (Invitrogen).

Flow cytometry analysis

To determine AQP7 expression, single-cell suspensions were stained with monoclonal antibodies (Abs) against CD11c, MHC class II, and EpCAM (eBioscience, San Diego, CA, USA) and were fixed in 4% formalin. Cells were permeabilized with 0.1% Triton X-100 and incubated with anti-AQP7 (Millipore) and a FITC-conjugated anti-rabbit IgG secondary antibody (Invitrogen). The samples were analyzed using a Fortessa flow cytometer (BD Biosciences, Franklin Lakes, NJ, USA). For the analysis of DCs, cell suspensions were stained with antibodies recognizing CD11c, MHC class II, EpCAM, CD80, CD86, CCR7, and CXCR4 (eBioscience). Information regarding antibodies is available in Supplemental Table S1.

Macropinocytosis and phagocytosis assay

Freshly isolated epidermal or dermal cell suspensions were incubated in cRPMI for 1 h, followed with a Lucifer yellow CH potassium salt (LY, 0.1 mg/ml; Sigma), fluorescein isothiocyanate (FITC; 0.1–1 mg/ml; Invitrogen), FITC-dextran (molecular mass ~4, 40, 250 kDa, 0.5 mg/ml; Sigma), or FITC-ovalbumin (FITC-OVA; 0.25 mg/ml; Invitrogen) in cRPMI for 45 min (37°C, 5% CO_2). The cells were washed 4 times with cold PBS containing 1% BSA, stained with anti-MHC class II, and analyzed on a flow cytometer.

Water and glycerol permeability of LCs

Water and glycerol permeability were measured using a SX20 stopped-flow spectrometer (Applied Photophysics, Surrey, UK). Isolated LCs in RPMI medium (1×10^6 cells/μl) were subjected to a 150 mM inwardly directed mannitol or glycerol gradient at 22°C. Water uptake was measured by the kinetics of the decrease in cell volume, as measured by the 90° scattered light intensity at a wavelength of 450 nm, over the time course (24, 25). Glycerol uptake was estimated by a single exponential fit on the second part of the curve, as described previously (26). Reciprocal exponential time constants (τ^{-1}) were calculated.

Chemotaxis assay

Epidermal or dermal cell suspensions (10^6 cell/100 μl) were deposited into the upper chamber of a polycarbonate transwell membrane filter (5 μm pore size; Corning Costar, Cambridge, MA, USA). The lower chamber contained CXCL12 (100 ng/ml) or CCL21 (100 ng/ml) in cRPMI medium. After incubation for 3 h at 37°C, the recovered cells were analyzed using flow cytometry.

Contact hypersensitivity

Mice were sensitized by application of 20 μl of 2,4-dinitrofluorobenzene (DNFB; 0.5%) solution on the abdomen. After 5 d, 20 μl of DNFB (0.3%) was applied to the left ear, and the vehicle (acetone/olive oil, 4:1) was applied to the right ear. Ear swelling was measured with a thickness gauge (Teclok, Nagano, Japan) at 24 h after challenge.

DNFB-dependent cell proliferation and cytokine production were examined with cells (5×10^5) isolated from the axillary and inguinal LNs at 5 d after sensitization. The LN cells were cultured in the absence or presence of trinitrochlorobenzene (TNCB; 50 μg/ml) for 3 d, pulsed with 0.5 μCi [^{3}H]-thymidine for 24 h, and subjected to liquid scintillation counting. IFN-γ release into the culture supernatant during the entire 3-d period was determined using an ELISA kit (eBioscience).

For the adoptive transfer, cell suspensions obtained from the LNs of DNFB-sensitized mice were injected subcutaneously (2×10^5 cells/20 μl PBS) into the ears of naive WT mice. The ears were immediately challenged by applying 20 μl of 0.3% DNFB or vehicle to either side of the ear. Ear thickness was measured after 24 h.

Antigen-induced cutaneous DC migration

Mice were painted with 200 μl FITC (10 mg/ml in acetone and dibutyl phthalate, 1:1; Invitrogen) or 100 μl FITC-OVA (2 mg/ml in 50% ethanol; Invitrogen), and the number of migrated cutaneous DCs in the draining LNs was analyzed by flow cytometry. Before application of FITC-OVA, the stratum corneum was removed by tape stripping (3 or 10 times) to disrupt the skin permeability barrier, and the transepidermal water loss (TEWL) value was monitored with a Tewameter Vapo Scan (Asahi Biomed, Tokyo, Japan) as an index of barrier function (Asahi Biomed, Tokyo, Japan).

Statistical analysis

Statistical analysis was performed using a 2-tailed Student's *t* test or ANOVA.

RESULTS

AQP7 expression in mouse cutaneous DCs

To characterize the expression of AQP7 in cutaneous DCs, we analyzed AQP7 expression levels in mouse DCs, including epidermal LCs and dermal DCs (dDCs). The epidermis and dermis were separated by dispase treatment and digested into single-cell suspensions by an enzyme-free cell dissociation buffer or collagenase treatment, respectively. CD11c$^+$ cells were selected by AutoMACS bead separation from freshly isolated, functionally immature cells, and we analyzed AQP7 mRNA levels by quantitative real-time RT-PCR. An AQP7 transcript was identified in both LCs and dDCs as well as in CD4$^+$ T cells (**Fig. 1*A***). We also found that AQP3 was expressed in LCs and dDCs, while we did not identify AQP5 and AQP9 expression in skin DCs, implying that skin DCs might have different expression patterns of AQPs from BMDCs (Supplemental Fig. S1).

Using a germline AQP7$^{-/-}$ mouse as a control (23), we verified the expression of AQP7 protein in MHC class II$^+$ CD11c$^+$ EpCAM$^+$ LC populations from the epidermal cell suspension by flow cytometry analysis (Fig. 1*B*). Immunofluorescence microscopy showed that AQP7 was mainly localized on the plasma membrane of CD11c$^+$ LCs (Fig. 1*C*).

To examine the function of AQP7 in the development of skin DCs, we analyzed the cell density and size of DCs isolated from the epidermis and dermis. We observed comparable cell numbers and cell size between wild-type (WT) and AQP7$^{-/-}$ mice, indicating that AQP7 deficiency does not affect the generation of LCs or dDCs (Fig. 1*D*).

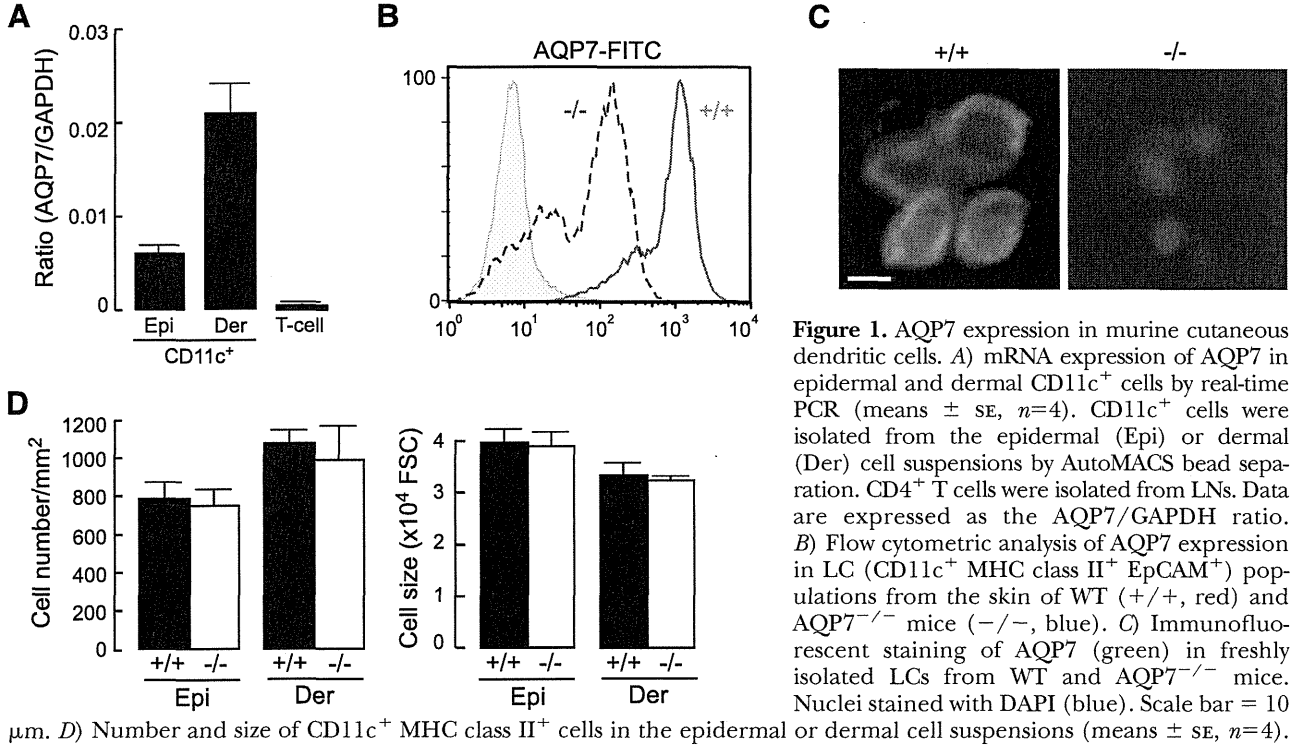

Figure 1. AQP7 expression in murine cutaneous dendritic cells. *A*) mRNA expression of AQP7 in epidermal and dermal CD11c$^+$ cells by real-time PCR (means ± SE, n=4). CD11c$^+$ cells were isolated from the epidermal (Epi) or dermal (Der) cell suspensions by AutoMACS bead separation. CD4$^+$ T cells were isolated from LNs. Data are expressed as the AQP7/GAPDH ratio. *B*) Flow cytometric analysis of AQP7 expression in LC (CD11c$^+$ MHC class II$^+$ EpCAM$^+$) populations from the skin of WT (+/+, red) and AQP7$^{-/-}$ mice (−/−, blue). *C*) Immunofluorescent staining of AQP7 (green) in freshly isolated LCs from WT and AQP7$^{-/-}$ mice. Nuclei stained with DAPI (blue). Scale bar = 10 μm. *D*) Number and size of CD11c$^+$ MHC class II$^+$ cells in the epidermal or dermal cell suspensions (means ± SE, n=4).

Impaired water/glycerol transport and antigen uptake in AQP7-deficient DCs

Previous studies using *Xenopus* oocytes expressing AQP7 found that AQP7 facilitates water and glycerol uptake (27, 28). We determined the osmotic water and glycerol permeability in isolated LCs from WT and AQP7$^{-/-}$ mice. The kinetics of the change in scattered light intensity in response to an osmotic challenge were measured as described previously (24, 25). Water transport in response to a 150 mM inwardly directed mannitol gradient was significantly higher in WT than in AQP7-deficient cells (**Fig. 2*A***). Glycerol permeability, measured by the stopped-flow technique, as described previously (26), was also decreased in the absence of AQP7 as compared to WT cells (Fig. 2*B*).

We next tested the hypothesis that AQP7 is involved in macropinocytosis and/or phagocytosis in DCs. First, we utilized FITC-labeled dextran, which is a commonly used model substance for pinocytosis and phagocytosis (6, 29). Epidermal or dermal cell suspensions were incubated with FITC-dextran, and the mean fluorescence intensity (MFI) of ingested FITC gated on MHC class II$^+$ cells was analyzed. Figure 2*C* shows that AQP7-deficient LCs had a reduced cellular uptake of FITC-dextran, which has components with molecular masses ranging from 4 to 250 kDa. In dDCs, AQP7 had an effect on the uptake of 4- to 40-kDa FITC-dextran molecules (Fig. 2*D*).

The FITC-dextran assay tests receptor-mediated endocytosis in the internalization of dextran because DCs express pattern recognition receptors that bind to carbohydrate moieties such as dextran (6, 29). We next utilized FITC and LY to more precisely examine macropinocytosis. Both FITC and LY uptake were significantly decreased in AQP7-deficient DCs compared to WT cells (Fig. 2*E, F*). These results indicate that AQP7 is involved in macropinocytosis in DCs.

Impaired chemotaxis in AQP7-deficient DCs

Immune responses are initiated when antigen-bearing DCs migrate from skin to LNs and activate T cells (3–5). Therefore, we examined the chemotaxis of skin DCs toward the ligands CXCL12 and CCL21 (30). Chemotaxis was significantly impaired in AQP7-deficient LCs and dDCs compared to WT cells (**Fig. 3*A***). The expression levels of the maturation markers CD80 and CD86 and of the chemokine receptors for migration, CCR7 and CXCR4, were comparable between WT and AQP7-deficient DCs (Fig. 3*B, C*). These findings suggested that AQP7 is involved not only in antigen uptake but also in the migration of DCs.

Because AQP7 was detected in CD4$^+$ T cells (Fig.

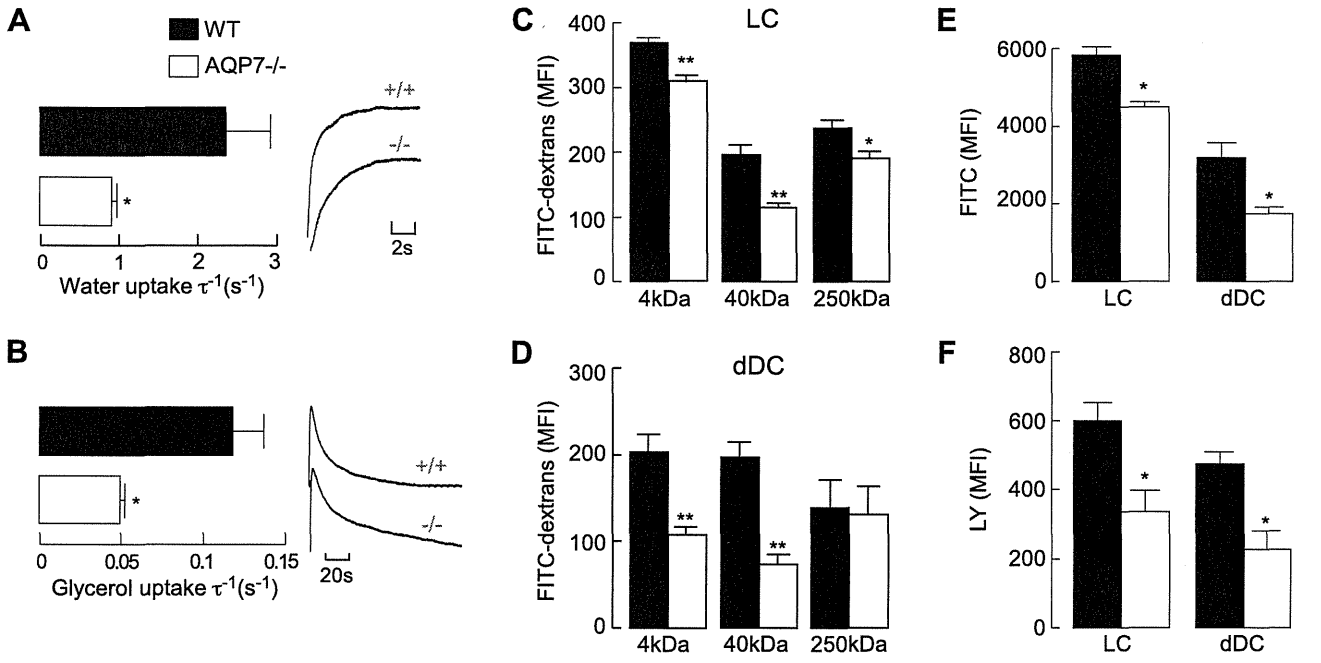

Figure 2. Impaired water/glycerol transport and macropinocytosis in AQP7-deficient DCs. *A*) Osmotic water permeability of LCs from WT and AQP7$^{-/-}$ mice was measured by scattered light intensity over the time course in response to a 150 mM inwardly directed mannitol gradient by stopped flow at 22°C. Reciprocal exponential time constant τ^{-1} was calculated (n=4). *$P < 0.01$. *B*) Glycerol permeability was measured in response to a 150 mM inward glycerol gradient by stopped flow at 22°C (n=4). *$P <$ 0.01. *C, D*) Cellular uptake of FITC-dextran. Epidermal (*C*) or dermal (*D*) cell suspensions were incubated with FITC-dextran (4, 40, or 250 kDa, 0.5 mg/ml) for 45 min at 37°C. Mean fluorescence intensity (MFI) of internalized FITC in MHC class II$^+$ cells was monitored (n=5). *$P < 0.05$, **$P < 0.01$. *E, F*) FITC (*E*) and LY (*F*) uptake by LCs and dDCs from WT and AQP7$^{-/-}$ mice. FITC or LY (0.1–1 mg/ml) was incubated in the cell suspension from the epidermis or dermis (45 min, 37°C). FITC or LY uptake was monitored by measuring the MFI of internalized FITC or LY in MHC class II$^+$ cells (n=4). *$P < 0.01$. Data are presented as means ± SE.

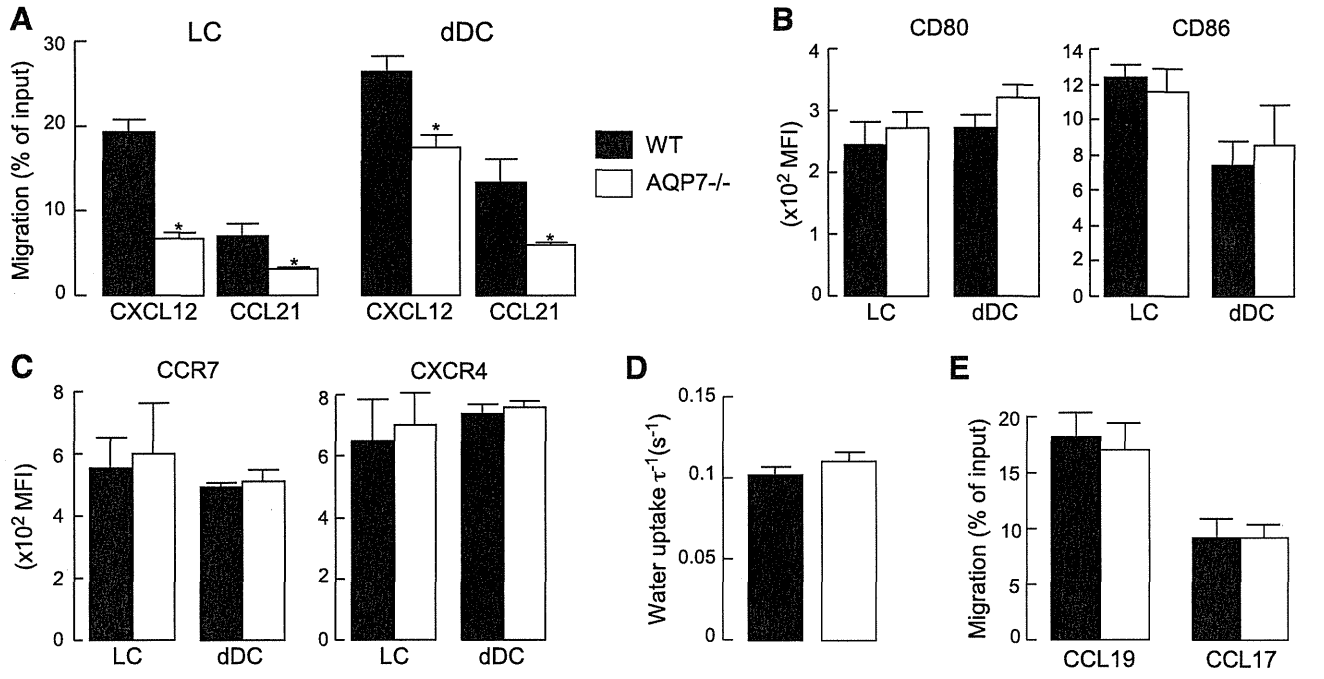

Figure 3. Impaired chemotaxis in AQP7-deficient DCs. *A*) Chemotaxis assay. Migration of DCs (epidermal or dermal cell suspensions) to the ligands CXCL12 (100 ng/ml) or CCL21 (100 ng/ml) was examined using a transwell chamber with 5-μm pores. Graphs show percentages of cells that migrated (n=5). *$P < 0.01$. *B, C*) Expression levels of maturation markers (*B*) and chemokine receptors involved in migration (*C*). Epidermal (for LCs) and dermal (for dDCs) cell suspensions were incubated in cRPMI for 2 d. MFI of CD80-APC$^+$, CD86-FITC$^+$, CCR7-PC7$^+$, and CXCR4-FITC$^+$ cells within the MHC class II$^+$ cell gate was determined (n=4). *D*) Osmotic water permeability in isolated CD4$^+$ T cells from WT and AQP7$^{-/-}$ mice (n=4). *E*) Chemotaxis assay of T cells. Migration of CD4$^+$ T cells to the ligands CCL19 (100 ng/ml) and CCL17 (100 ng/ml) was examined using a transwell chamber with 5-μm pores. Graphs show percentages of cells that migrated (n=5). Data are presented as means ± SE.

1*A*), we conducted a phenotypic analysis of T cells in the spleen, LNs, and thymus. CD4$^+$ and CD8$^+$ lymphocyte numbers (Supplemental Fig. S2) and the cell populations of CD3, CD25, CD44, and CD62L (not shown) in the LNs and thymus were similar between WT and AQP7-deficient mice. The water permeability of CD4$^+$ T cells (Fig. 3*D*) and chemotaxis toward CD4$^+$ T-cell ligands (Fig. 3*E*) were also comparable between WT and AQP7-deficient T cells, indicating that the expression of AQP7 likely has little effect on T-cell development or function.

Impaired OVA-induced sensitization in AQP7$^{-/-}$ mice

We next investigated the effect of AQP7-mediated antigen uptake and cell migration on antigen-induced sensitization. Here we utilized FITC-labeled OVA. OVA is the main protein in egg whites and is an established model allergen. Fluorescence microscopy showed the cellular uptake of FITC-OVA in LCs after a 1-h incubation (**Fig. 4*A***, left panel). Flow cytometry analysis demonstrated that AQP7-deficient LCs and dDCs had impaired incorporation of FITC-OVA (Fig. 4*A*, right panel).

We next sought to determine whether AQP7 has a role in antigen entry into the body, a process required for sensitization. To examine the effect of AQP7 deficiency on the response to the application of OVA on skin lesions, such as atopic dermatitis, the skin permeability barrier was disrupted by tape stripping (3 or 10 times) to remove the stratum corneum, and FITC-OVA was applied. The TEWL values of WT and AQP7$^{-/-}$ skin were comparable after tape stripping, indicating that barrier disruption occurred equally (Fig. 4*B*, left panel). The numbers of FITC$^+$ LCs and dDCs that migrated into the LNs were significantly impaired in AQP7$^{-/-}$ mice compared to WT mice (Fig. 4*B*, right panel). We next examined sensitization to OVA. We isolated a similar number of lymphocytes from the draining LNs of WT and AQP7$^{-/-}$ mice at 48 h after applying FITC-OVA, and the lymphocytes were incubated with OVA for 2 d. As shown in Fig. 4*C*, OVA-specific cell proliferation, as measured by [^{3}H]-thymidine incorporation, was impaired in AQP7-deficient cells compared to WT cells. These findings suggest that AQP7 is essential for antigen entry into the LNs following antigen-induced sensitization.

To investigate the involvement of AQP7 in antigen entry into the LNs using a different system, we utilized a FITC sensitization model wherein a FITC solution is applied to the skin, and cutaneous DCs take up FITC and migrate to the LNs for antigen presentation. Analysis of the skin-draining regional LNs at 24 h after FITC application showed a decrease in the accumulation of FITC$^+$ LCs and dDCs in AQP7$^{-/-}$ mice com-

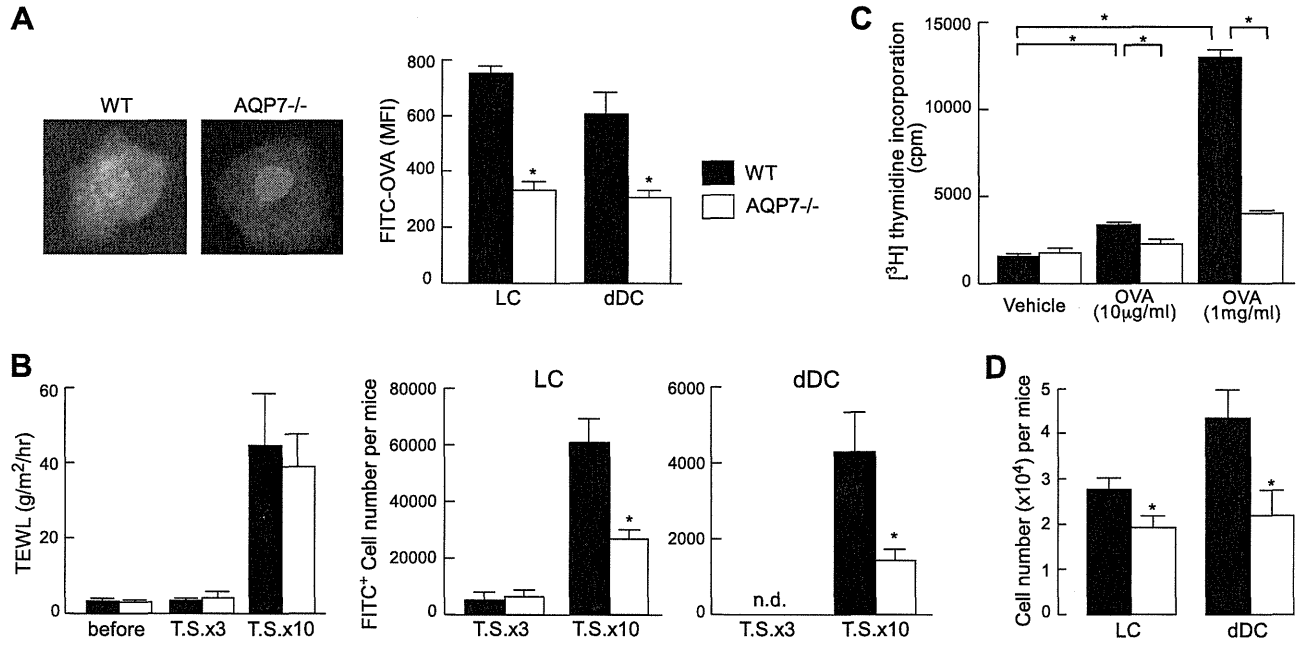

Figure 4. Impaired OVA-induced sensitization in AQP7$^{-/-}$ mice. *A*) Left panel: immunofluorescence microscopy of LCs incubated with FITC-OVA for 1 h at 37°C. Nuclei were stained with DAPI (blue). Right panel: cellular uptake of FITC-OVA. Epidermal or dermal cell suspensions were incubated with FITC-OVA (0.25 mg/ml) for 45 min at 37°C. MFI of internalized FITC was monitored (n=4). *B*) FITC-OVA migration *in vivo*. Skin permeability barrier was disrupted by tape stripping to remove the stratum corneum (3 or 10 times), and FITC-OVA was applied (100 μl of 2 mg/ml, 2×2 cm^2). Left panel: TEWL was measured as an index of barrier function after tape stripping. (Right panel: numbers of migrated LCs (CD11c$^+$ MHC class II$^+$ EpCAM$^+$) and dDCs (CD11c$^+$ MHC class II$^+$ EpCAM$^-$) 48 h after applying FITC-OVA (n=4). *C*) Antigen-specific cell proliferation was measured by [^{3}H]-thymidine incorporation. Lymphocytes (1×10^5 cells) isolated from the regional LNs of mice onto which FITC-OVA had been applied were incubated with vehicle or OVA (10 μg or 1 mg/ml) for 2 d (n=6). *D*) Skin DC migration into the draining LNs after FITC painting. WT and AQP7$^{-/-}$ mice were painted with 1% FITC solution (acetone and dibutylphthalate, 1:1) on the flank skin. At 24 h, LN cells were analyzed for the number of LCs (CD11c$^+$ MHC class II$^+$ EpCAM$^+$) or dDCs (CD11c$^+$ MHC class II$^+$ EpCAM$^-$) among FITC$^+$ cells by flow cytometry (n=5). Data are presented as means ± SE. *$P < 0.01$.

pared to WT mice (Fig. 4*D*). These data suggest the involvement of AQP7 in the induction of the primary immune response.

Impaired hapten-induced contact hypersensitivity and sensitization in AQP7$^{-/-}$ mice

To further determine the role of AQP7 in cutaneous immune reactions, we utilized a well-established hapten-induced contact hypersensitivity (CHS) model (31, 32). The WT and AQP7$^{-/-}$ mice were sensitized by applying DNFB to the abdomen, and the mice were challenged on the ear 5 d later. Ear swelling in response to the challenge, evidence of CHS, was significantly decreased in AQP7$^{-/-}$ mice compared to WT mice (**Fig. 5*A***). Histological examination confirmed that edema and the infiltration of lymphocytes into the dermis were attenuated in AQP7$^{-/-}$ mice, whereas these measures of inflammation were pronounced in WT skin (Fig. 5*A*, bottom panel).

To examine sensitization during the CHS response, antigen-specific cell proliferation and IFN-γ production were assayed. The lymphocytes from the draining LNs of WT and AQP7$^{-/-}$ mice were isolated at 5 d after DNFB sensitization, and the lymphocyte responses to TNCB, a water-soluble compound with the same antigenicity as DNFB, were compared *in vitro*. We observed a significant repression of antigen-induced cell proliferation and IFN-γ production in cells from AQP7$^{-/-}$ mice, indicating that T-cell activation during the sensitization period is impaired in the AQP7$^{-/-}$ mice.

Finally, we verified the impaired sensitization in AQP7$^{-/-}$ mice using subcutaneous adoptive transfer experiments. LN cells from sensitized WT and AQP7$^{-/-}$ mice were injected subcutaneously into the ears of naive recipient WT mice, which were challenged immediately with DNFB. As shown in Fig. 5*C*, the injected AQP7$^{-/-}$ cells suppressed ear swelling, and WT cells induced a strong CHS response. Collectively, these findings provide evidence that AQP7 expression is required for antigen-induced sensitization during the CHS response and that AQP7 might be responsible for antigen entry into the body.

DISCUSSION

Here we found that AQP7 is functionally expressed in skin DCs and is required for initiating cutaneous immune responses, such as CHS. An assay of macropinocytosis and/or phagocytosis showed that AQP7 defi-

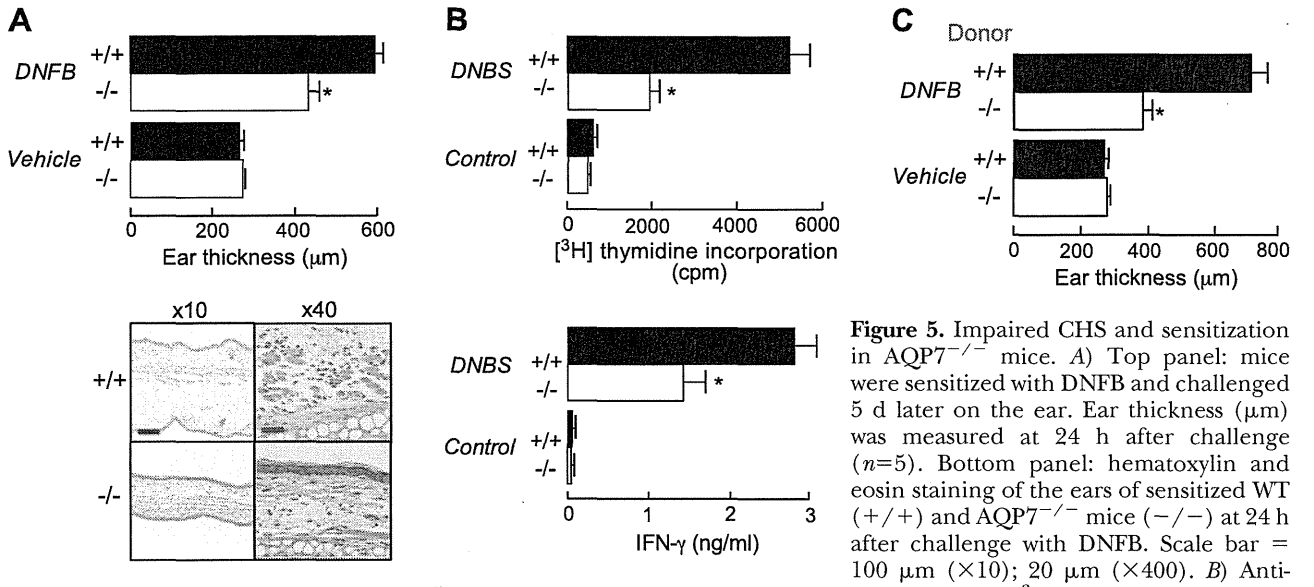

Figure 5. Impaired CHS and sensitization in AQP7$^{-/-}$ mice. *A*) Top panel: mice were sensitized with DNFB and challenged 5 d later on the ear. Ear thickness (μm) was measured at 24 h after challenge (n=5). Bottom panel: hematoxylin and eosin staining of the ears of sensitized WT (+/+) and AQP7$^{-/-}$ mice (−/−) at 24 h after challenge with DNFB. Scale bar = 100 μm (×10); 20 μm (×400). *B*) Antigen-specific cell proliferation (top panel) and IFN-γ production (bottom panel) during CHS. [^{3}H]-thymidine incorporation and IFN-γ production were determined in lymphocytes (1×10^5 cells) isolated from the regional LNs of DNFB-sensitized WT and AQP7$^{-/-}$ mice (n=5). *C*) Adoptive transfer experiments by subcutaneous injection. LN cells from sensitized donor WT and AQP7$^{-/-}$ mice (donor) were injected subcutaneously (2×10^5 cells) into the ear of naive recipient WT mice. Graph quantifies ear swelling at 24 h after challenge (n=4). Data are presented as means ± SE. *$P < 0.01$.

ciency decreased the cellular uptake of LY, FITC, FITC-OVA, and FITC-dextran into the skin DCs, including LCs and dDCs, suggesting the involvement of AQP7 in the capture of antigen. We also observed reduced cell migration toward ligands in AQP7-deficient DCs. In addition, AQP7$^{-/-}$ mice exhibited impaired antigen-induced sensitization after OVA or hapten application, and this impaired response was accompanied by suppressed lymphocyte proliferation. After application of a fluorescent antigen (FITC or FITC-OVA), the accumulation of antigen-retaining DCs in the LNs was decreased in AQP7$^{-/-}$ mice, which could be attributed to both the reduced captured of antigen and the reduced cell migration from skin to the LNs. Our findings provide the first evidence of the requirement for AQP7 in antigen-induced sensitization during an immune response.

DCs are antigen-presenting cells and are critical for the induction of primary immune responses. A previous study using human DCs derived from PBMCs showed that a mercury drug, one of the AQP inhibitors, blocked the macropinocytosis of LY but did not affect receptor-mediated endocytosis of FITC-dextran *via* the mannose receptor, suggesting that AQPs have a selective effect on macropinocytosis (20). In the study presented here, we demonstrated that AQP7 is involved in the cellular uptake of LY (MW 521), FITC (MW 389), FITC-conjugated dextran (MW ranging from 4 to 40 kDa), and FITC-OVA (MW ~45 kDa) into both LCs and dDCs, although it remains to be determined whether macropinocytosis, phagocytosis, or endocytosis was responsible for the uptake of these molecules. DCs express pattern-recognition receptors and bind to glycoproteins and other carbohydrate regions that are commonly expressed by pathogens (6, 33). Although the internalization of a soluble carbohydrate such as dextran into DCs occurs largely through receptor-mediated internalization, the assay using LY or FITC is thought to accurately examine macropinocytosis (6, 29). Therefore, our findings demonstrate that AQP7 is involved at least in macropinocytosis by skin DCs. After the intake of extracellular fluids by macropinocytosis, macrosolutes are concentrated and accumulate in a lysosomal compartment, which might depend on the selective transport of ions and water. We also demonstrated that AQP7 is required for water transport in DCs. AQP7-mediated water efflux might be responsible for regulating cell volume during macropinocytosis. Although further experiments are necessary to investigate the mechanism of AQP7-mediated antigen uptake, our data support the involvement of AQP7 in macropinocytosis.

In our studies, AQP7 was required for the chemotaxis of DCs, which might be important for antigen presentation and the subsequent initiation of the immune response. Previous studies have shown the involvement of some AQPs (AQP1, 3, and 4) in cell migration, for example, in angiogenesis or wound healing, in several endothelial and epithelial cell types (34, 35). The researchers of these studies proposed that AQP-mediated water transport was connected to actin dynamics during cell migration, although the cellular and molecular mechanisms that underlie this process are unclear. Again, macropinocytosis was found to be an actin-dependent process that requires the Rho-family GTPases, including Rac1 and Cdc42, for actin cytoskeletal rearrangements (33, 36). AQP7 might regulate the dynamics of actin reorganization, which regulates cell migration and macropinocytosis, and future studies will define the mechanism of AQP7-mediated DC migration.

In summary, our data provide the first evidence that AQP7 is required for the induction of primary cutane-

ous immune responses. Our findings suggest that AQP7 is primarily involved in antigen uptake and subsequently in the migration of epidermal LCs and dDCs, which are responsible for antigen processing and presentation and promote immune responses. Because DCs are localized not only in the skin but in most tissues of the body, AQP7 might have a causal role in allergy or unwanted immune reactions. Our findings suggest that blocking AQP7 by the use of topical drugs might be useful for the suppression of undesirable immune responses. FJ

The authors thank Maiko Yusa and Kiiko Kumagai for mouse breeding, Dr. Yoshinori Fujiyoshi and Akiko Kamegawa for help with water transport measurement, and Dr. Shunsuke Chikuma for critical reading of the manuscript. This work was supported in part by grants from the Ministry of Education, Culture, Sports, Science, and Technology of Japan.

REFERENCES

1. Merad, M., Ginhoux, F., and Collin, M. (2008) Origin, homeostasis and function of Langerhans cells and other langerin-expressing dendritic cells. *Nat. Rev. Immunol.* **8,** 935–947
2. Romani, N., Clausen, B. E., and Stoitzner, P. (2010) Langerhans cells and more: langerin-expressing dendritic cell subsets in the skin. *Immunol. Rev.* **234,** 120–141
3. Kripke, M. L., Munn, C. G., Jeevan, A., Tang, J. M., and Bucana, C. (1990) Evidence that cutaneous antigen-presenting cells migrate to regional lymph nodes during contact sensitization. *J. Immunol.* **145,** 2833–2838
4. Banchereau, J., Briere, F., Caux, C., Davoust, J., Lebecque, S., Liu, Y. J., Pulendran, B., and Palucka, K. (2000) Immunobiology of dendritic cells. *Annu. Rev. Immunol.* **18,** 767–811
5. Randolph, G. J., Angeli, V., and Swartz, M. A. (2005) Dendritic-cell trafficking to lymph nodes through lymphatic vessels. *Nat. Rev. Immunol.* **5,** 617–628
6. Norbury, C. C. (2006) Drinking a lot is good for dendritic cells. *Immunology* **117,** 443–451
7. Savina, A., and Amigorena, S. (2007) Phagocytosis and antigen presentation in dendritic cells. *Immunol. Rev.* **219,** 143–156
8. Noordegraaf, M., Flacher, V., Stoitzner, P., and Clausen, B. E. (2010) Functional redundancy of Langerhans cells and Langerin+ dermal dendritic cells in contact hypersensitivity. *J. Invest. Dermatol.* **130,** 2752–2759
9. Honda, T., Nakajima, S., Egawa, G., Ogasawara, K., Malissen, B., Miyachi, Y., and Kabashima, K. (2010) Compensatory role of Langerhans cells and langerin-positive dermal dendritic cells in the sensitization phase of murine contact hypersensitivity. *J. Allergy Clin. Immunol.* **125,** 1154–1156
10. Rojek, A., Praetorius, J., Frøkiaer, J., Nielsen, S., and Fenton, R. A. (2008) A current view of the mammalian aquaglyceroporins. *Annu. Rev. Physiol.* **70,** 301–327
11. Verkman, A. S. (2009) Aquaporins: translating bench research to human disease. *J. Exp. Biol.* **212,** 1707–1715
12. Carbrey, J. M., and Agre, P. (2009) Discovery of the aquaporins and development of the field. *Handb. Exp. Pharmacol.* **190,** 3–28
13. Savage, D. F., Egea, P. F., Robles-Colmenares, Y., O'Connell, JD, 3rd, and Stroud, R. M. (2003) Architecture and selectivity in aquaporins: 2.5 a X-ray structure of aquaporin Z. *PLoS Biol.* **1,** E72
14. Oliva, R., Calamita, G., Thornton, J. M., and Pellegrini-Calace, M. (2010) Electrostatics of aquaporin and aquaglyceroporin channels correlates with their transport selectivity. *Proc. Natl. Acad. Sci. U. S. A.* **107,** 4135–4140
15. Verkman, A. S. (2008) Dissecting the roles of aquaporins in renal pathophysiology using transgenic mice. *Semin. Nephrol.* **28,** 217–226
16. Saadoun, S., Papadopoulos, M. C., Hara-Chikuma, M., and Verkman, A. S. (2005) Impairment of angiogenesis and cell migration by targeted aquaporin-1 gene disruption. *Nature* **434,** 786–792
17. Hara-Chikuma, M., and Verkman, A. S. (2008) Prevention of skin tumorigenesis and impairment of epidermal cell proliferation by targeted aquaporin-3 gene disruption. *Mol. Cell. Biol.* **28,** 326–332
18. Lennon, V. A., Kryzer, T. J., Pittock, S. J., Verkman, A. S., and Hinson, S. R. (2005) IgG marker of optic-spinal multiple sclerosis binds to the aquaporin-4 water channel. *J. Exp. Med.* **202,** 473–477
19. Papadopoulos, M. C., and Verkman, A. S. (2007) Aquaporin-4 and brain edema. *Pediatr. Nephrol.* **22,** 778–784
20. De Baey, A., and Lanzavecchia, A. (2000) The role of aquaporins in dendritic cell macropinocytosis. *J. Exp. Med.* **191,** 743–748
21. Moon, C., Rousseau, R., Soria, J. C., Hoque, M. O., Lee, J., Jang, S. J., Trink, B., Sidransky, D., and Mao, L. (2004) Aquaporin expression in human lymphocytes and dendritic cells. *Am. J. Hematol.* **75,** 128–133
22. Wang, G. F., Dong, C. L., Tang, G. S., Shen, Q., and Bai, C. X. (2008) Membrane water permeability related to antigen-presenting function of dendritic cells. *Clin. Exp. Immunol.* **153,** 410–419
23. Sohara, E., Rai, T., Miyazaki, J., Verkman, A. S., Sasaki, S., and Uchida, S. (2005) Defective water and glycerol transport in the proximal tubules of AQP7 knockout mice. *Am. J. Physiol. Renal Physiol.* **289,** F1195–F2000
24. Yang, B., Kim, J. K., and Verkman, A. S. (2006) Comparative efficacy of HgCl2 with candidate aquaporin-1 inhibitors DMSO, gold, *TEA+*, and acetazolamide. *FEBS Lett.* **580,** 6679–6684
25. Tanimura, Y., Hiroaki, Y., and Fujiyoshi, Y. (2009) Acetazolamide reversibly inhibits water conduction by aquaporin-4. *J. Struct. Biol.* **166,** 16–21
26. Roudier, N., Verbavatz, J. M., Maurel, C., Ripoche, P., and Tacnet, F. (1998) Evidence for the presence of aquaporin-3 in human red blood cells. *J. Biol. Chem.* **273,** 8407–8412
27. Ishibashi, K., Kuwahara, M., Gu, Y., Kageyama, Y., Tohsaka, A., Suzuki, F., Marumo, F., and Sasaki, S. (1997) Cloning and functional expression of a new water channel abundantly expressed in the testis permeable to water, glycerol, and urea. *J. Biol. Chem.* **272,** 20782–20786
28. Kuriyama, H., Kawamoto, S., Ishida, N., Ohno, I., Mita, S., Matsuzawa, Y., Matsubara, K., and Okubo, K. (1997) Molecular cloning and expression of a novel human aquaporin from adipose tissue with glycerol permeability. *Biochem. Biophys. Res. Commun.* **241,** 53–58
29. Sallusto, F., Cella, M., Danieli, C., and Lanzavecchia, A. (1995) Dendritic cells use macropinocytosis and the mannose receptor to concentrate macromolecules in the major histocompatibility complex class II compartment: downregulation by cytokines and bacterial products. *J. Exp. Med.* **182,** 389–400
30. Dieu-Nosjean, M. C., Vicari, A., Lebecque, S., and Caux, C. (1999) Regulation of dendritic cell trafficking: a process that involves the participation of selective chemokines. *J. Leukoc. Biol.* **66,** 252–262
31. Grabbe, S., and Schwarz, T. (1998) Immunoregulatory mechanisms involved in elicitation of allergic contact hypersensitivity. *Immunol. Today* **19,** 37–44
32. Martin, S. F. (2004) T lymphocyte-mediated immune responses to chemical haptens and metal ions: implications for allergic and autoimmune disease. *Int. Arch. Allergy Immunol.* **134,** 186–198
33. Kerr, M. C., and Teasdale, R. D. (2009) Defining macropinocytosis. *Traffic* **10,** 364–371
34. Papadopoulos, M. C., Saadoun, S., and Verkman, A. S. (2008) Aquaporins and cell migration. *Pflügers Arch.* **456,** 693–700
35. Hara-Chikuma, M., and Verkman, A. S. (2008) Aquaporin-3 facilitates epidermal cell migration and proliferation during wound healing. *J. Mol. Med.* **86,** 221–231
36. West, M. A., Prescott, A. R., Eskelinen, E. L., Ridley, A. J., and Watts, C. (2000) Rac is required for constitutive macropinocytosis by dendritic cells but does not control its downregulation. *Curr. Biol.* **10,** 839–488

Received for publication April 19, 2011.
Accepted for publication September 15, 2011.

Biochemical and Biophysical Research Communications 425 (2012) 456–461

Contents lists available at SciVerse ScienceDirect

Biochemical and Biophysical Research Communications

journal homepage: www.elsevier.com/locate/ybbrc

Phosphorylation of Na–Cl cotransporter by OSR1 and SPAK kinases regulates its ubiquitination

Muhammad Zakir Hossain Khan, Eisei Sohara *, Akihito Ohta, Motoko Chiga, Yuichi Inoue, Kiyoshi Isobe, Mai Wakabayashi, Katsuyuki Oi, Tatemitsu Rai, Sei Sasaki, Shinichi Uchida

Department of Nephrology, Graduate School of Medicine, Tokyo Medical and Dental University, 1-5-45 Yushima, Bunkyo-ku, Tokyo 113-8519, Japan

ARTICLE INFO

Article history:
Received 11 July 2012
Available online 27 July 2012

Keywords:
Na–Cl cotransporter
Phosphorylation
Ubiquitination
Pseudohypoaldosteronism type II
Dietary salt

ABSTRACT

Na–Cl cotransporter (NCC) is phosphorylated in its amino terminus based on salt intake under the regulation of the WNK-OSR1/SPAK kinase cascade. We have observed that total protein abundance of NCC and its apical membrane expression varies in the kidney based on the phosphorylation status. To clarify the mechanism, we examined NCC ubiquitination status in mice fed low, normal and high salt diets, as well as in a model mouse of pseudohypoaldosteronism type II (PHAII) where NCC phosphorylation is constitutively elevated. Low-salt diet decreased NCC ubiquitination, while high-salt diet increased NCC ubiquitination in the kidney, and this was inversely correlated with total and phosphorylated NCC abundance. In the PHAII model, the ubiquitination of NCC in kidney was also lower when compared to that in wild-type littermates. To evaluate the relationship between phosphorylation and ubiquitination of NCC, we expressed wild-type, phospho-deficient and -mimicking NCC in COS7 cells, and the ubiquitination of immunoprecipitated total and biotinylated surface NCC was evaluated. NCC ubiquitination was increased in the phospho-deficient NCC and decreased in phospho-mimicking NCC in both total and surface NCC. Thus, we demonstrated that NCC phosphorylation decreased NCC ubiquitination, which may contribute to the increase of NCC abundance mostly on plasma membranes.

1. Introduction

The thiazide-sensitive NaCl cotransporter (NCC) is essential for sodium reabsorption at the distal convoluted tubules (DCT) in the kidney. A loss-of-function NCC mutation causes Gitelman's syndrome, an inherited disease that exhibits salt-losing phenotypes [1]. In contrast, a gain-of-function mutation in NCC causes pseudohypoaldosteronism type II (PHAII), a disease of salt-sensitive hypertension. PHAII was shown to be caused by mutations in the with-no-lysine kinases 1 and 4 (WNK1 and WNK4) [2], and we clarified using a PHAII model mouse (*Wnk4*$^{D561A/+}$) that the pathogenesis of PHAII was the constitutive activation of a phosphorylation signal cascade consisting of WNK kinase, oxidative stress-responsive kinase-1 (OSR1), STE20/SPS1-related proline/alanine-rich kinase (SPAK), and NCC [3].

NCC is phosphorylated at several amino-terminal serine and threonine residues (T53, T58 and S71 in mouse NCC) by OSR1/SPAK [4], which is highly elevated in *Wnk4*$^{D561A/+}$ knock-in mice [3]. SPAK knockout mice showed decreased phosphorylation of NCC at these sites and exhibit Gitelman's syndrome-like phenotypes [5], thus confirming the importance of NCC phosphorylation in the *in vivo* function of NCC. Pacheco-Arevarez et al. showed that the phosphorylation of NCC is important for its transport function when expressed in *Xenopus* oocytes [6]. In addition to this mechanism, it was observed that phosphorylated NCC was concentrated on the plasma membranes of DCT, thus suggesting that phosphorylation is involved in the accumulation of NCC in plasma membranes [7,8].

We recently reported several physiological regulators of NCC phosphorylation. NCC phosphorylation is increased by a low-salt diet through aldosterone [9]. Angiotensin II and insulin were found to increase NCC phosphorylation [10–13]. Interestingly, total protein abundance of NCC appeared to vary according to NCC phosphorylation in these cases. Similar phenomena were also observed in *Wnk4*$^{D561A/+}$ knock-in, SPAK knockout, SPAK and OSR1 knock-in mice [3,5,14], thus suggesting that NCC phosphorylation is able to regulate its total protein abundance mostly on plasma membranes. However, the underlying mechanisms of how phosphorylation of NCC increases surface expression have yet to be clarified.

Numerous membranous proteins, including various ion transporters of the kidney, have been shown to be degraded in a regulated manner that involves ubiquitination. For example, epithelial sodium channel (ENaC) is ubiquitinated by Nedd4-2, and ubiquitinated ENaC is sorted to a degradation pathway [15]. Impaired ENaC ubiquitination at the cell surface by the mutation of ENaC in Liddle

* Corresponding author. Fax: +81 3 5803 5215.
E-mail address: esohara.kid@tmd.ac.jp (E. Sohara).

0006-291X/$ - see front matter © 2012 Elsevier Inc. All rights reserved.
http://dx.doi.org/10.1016/j.bbrc.2012.07.124

syndrome results in increased ENaC protein levels at the cell surface, leading to increased sodium reabsorption and hypertension [16,17]. In the case of NCC, it has been reported that NCC is polyubiquitinated in its secretory pathway (ER) and undergoes proteasomal degradation [18]. It has also been reported that ubiquitin ligase Nedd4-2 ubiquitinates NCC [19]. These observations suggest that NCC phosphorylation and ubiquitination are coordinated and involved in the regulation of NCC under various pathophysiological conditions.

In this study, we found that dietary salt intake regulates NCC ubiquitination and phosphorylation *in vivo*. Similarly, NCC ubiquitination was decreased in a PHAII mouse model. In addition, we clarified that NCC phosphorylation regulates NCC ubiquitination. Thus, ubiquitination of NCC may be an important determinant of NCC protein abundance and plasma membrane localization within cells.

2. Materials and methods

2.1. Animal study

C57BL/6 mice (age, 12 weeks) were fed normal diet, low-NaCl diet (0.01% NaCl (w/w)) or high-NaCl diet (4% NaCl (w/w)) for 14 days. *Wnk4*$^{+/+}$ and *Wnk4*$^{D561A/+}$ mice were fed normal diet. All animal procedures were approved by the Institutional Animal Care and Use Committee of the Tokyo Medical and Dental University.

2.2. Immunoprecipitation of NCC from mouse kidney

Mice were sacrificed after 14 days on the diet. Whole kidneys were homogenized in homogenization buffer (250 mM sucrose, 10 mM triethanolamine, 1 mM EGTA, 1 mM EDTA, 20 mM *N*-ethylmaleimide (NEM), 50 mM sodium fluoride, 1 mM sodium orthovanadate and complete protease inhibitor). Isolated crude membrane fraction (17,000g) was solubilized in buffer SB (0.5% sodium-deoxycholate, 20 mM Tris HCl, 5 mM EDTA, 10% glycerol and complete protease inhibitor). Samples were precleared by incubating with immobilized protein G, and were then subjected to NCC immunoprecipitation by rabbit anti-NCC antibody (Chemicon, Temecula, CA, USA). As a negative control, samples were incubated with rabbit IgG.

2.3. Plasmids

Full-length wild-type T7-tagged NCC and T7-tagged phospho-deficient NCC expression plasmid (pRK5-T7-tagged NCC and pRK5-T7-tagged NCC) was kindly provided by Dr. T. Moriguchi [20]. T7-tagged phospho-mimicking NCC (pRK5-T7-tagged NCC) was generated by site-directed mutagenesis with using the QuikChange Mutagenesis system (Stratagene, La Jolla, CA, USA).

2.4. Cell culture and transient transfection

COS7 cells were grown in low bicarbonate Dulbecco's modified Eagle's medium supplemented with 10% (v/v) fetal calf serum. Cells were transfected with 8 μg of each plasmid using Lipofectamine 2000 (Invitrogen, CA, USA).

2.5. Immunoprecipitation of transiently expressed NCC in COS7 cell

Empty vector (PRK-5), T7-tagged phospho-deficient, wild-type or phospho-mimicking NCC was transfected into COS7 cells. At 48 h after transfection, cells were lysed with buffer M-PER (Thermo Scientific, Massachusetts, USA) containing 20 mM NEM and complete protease inhibitor. Lysates were centrifuged at 17,000g for 30 min. Supernatant was precleared with immobilized protein G, and was then subjected to NCC immunoprecipitation by rabbit anti-NCC antibody bound to protein A-Sepharose beads.

2.6. Cell surface biotinylation assay

COS7 cells were transfected with empty vector (PRK-5), T7-tagged phospho-deficient, wild-type or phospho-mimicking NCC. Cell surface proteins were labeled with sulfo-NHS (*N*-hydroxysuccinimido)-SS-biotin (Thermo Scientific) at 48 h after transfection as follows: cells were washed three times with PBS-CM (PBS with 1 mM $MgCl_2$ and $CaCl_2$). Cells were incubated for 30 min on ice with 0.5 mg/ml sulfo-NHS-SS-biotin in PBS-CM, and were then quenched with 100 mM glycine in PBS-CM. After washing three times with PBS-CM, cells were lysed in buffer M-PER (Thermo Scientific) containing 20 mM NEM and complete protease inhibitor. Lysates were centrifuged at 17,000g for 30 min. For pull down of total surface protein, lysates were incubated with immobilized NeutrAvidin beads (Pierce) at 4 °C for 2 h. For pull down of cell surface NCC, lysates were precleared with immobilized protein G, and were then subjected to the NCC immunoprecipitation by rabbit anti-NCC antibody (Chemicon, Temecula, CA, USA). NCC immune complexes bound to the protein A-Sepharose beads were eluted by boiling for 15 min in 100 μl of 1% SDS in PBS (pH 7.2) and diluted with 900 μl of PBS (pH 7.2). The solution was then incubated for 1 h at 4 °C with immobilized NeutrAvidin beads (Thermo Scientific) to isolate the biotinylated NCC surface fraction.

2.7. Immunoblotting

Semi-quantitative immunoblotting was performed, as described previously [21,22]. To assess relative expression levels of proteins in whole kidney, homogenates without the nuclear fraction (600g) or the crude membrane fraction (17,000g) were used. Band intensity was analyzed using Image J (NIH, Betheda, MD, USA). To quantify ubiquitinated protein signals from immunoblots, we calculated the amount of protein (in arbitrary units) from a 6-fold dilution series of the same protein that was also immunoblotted. The following primary antibodies were used in this study: rabbit total anti-NCC [23]; guinea pig total anti-NCC [23]; rabbit anti-pNCC (T53, T58 and S71) [9]; anti-T7 (from Invitrogen); and mouse anti-ubiquitin (Santa Cruz Biotechnology, CA, USA). Alkaline-phosphatase-conjugated anti-IgG antibodies (Promega, Madison, WI, USA) were used as secondary antibodies for immunoblotting.

2.8. Statistical analysis

Statistical significance was evaluated by unpaired *t*-test. All data are expressed as mean ± SEM. When more than three groups were compared, one-way ANOVA with Fischer's post hoc test was used. $P < 0.05$ was considered to be statistically significant.

3. Results

3.1. Dietary salt regulates ubiquitination of NCC in mouse kidney

In order to investigate whether ubiquitination of NCC is involved in the regulation of its abundance in the kidney, we examined NCC ubiquitination in the kidney from mice under various dietary salt intake conditions. As shown in Fig. 1A, NCC protein abundance and phosphorylation were increased under a low-salt diet and decreased under a high-salt diet, as reported previously [9]. NCC ubiquitination was then evaluated under the same conditions. As shown in Fig. 1A and B, ubiquitination of NCC was significantly elevated and reduced in kidneys from mice fed high-salt and low-salt diets, respectively.

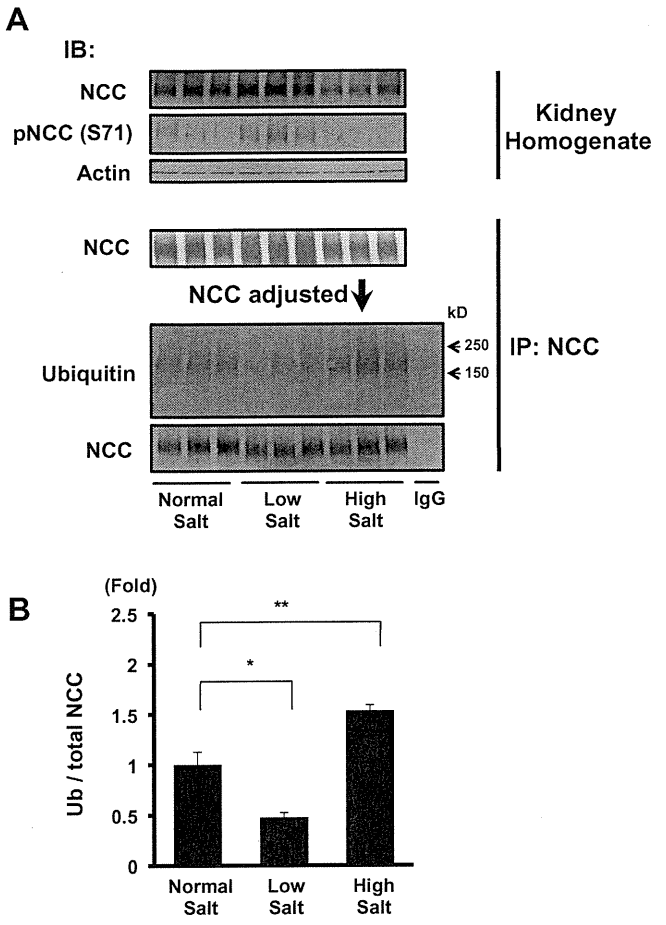

Fig. 1. Ubiquitination of NCC is regulated by dietary salt intake. (A) Immunoblots of total and phosphorylated NCC in the kidneys of wild-type mice fed diets with different amounts of salt. NCC Phosphorylation at S71 was regulated by different amounts of salt in the diet; phosphorylation and abundance of NCC decreased under a high-salt diet and increased under a low-salt diet (upper panels). NCC was immunoprecipitated from kidney homogenates of mice fed diets containing different amounts of salt. Immunoprecipitated NCC was adjusted to have nearly equal amounts of immunoprecipitated NCC in each lane in order to more clearly demonstrate the differences in ubiquitination in each lane (lower panel). Immunoprecipitated NCC was blotted with ubiquitin antibody. NCC ubiquitination was lower in mice fed low-salt diet and higher in mice fed high-salt diet, as compared to mice fed normal diet. (B) Densitometry analysis of ubiquitination of immunoprecipitated NCC in mice fed different amounts of salt. For densitometry analysis, values are expressed as ratios of ubiquitinated and total NCC against mean signals in the normal diet group. $^{**}P < 0.01$, $^{*}P < 0.05$.

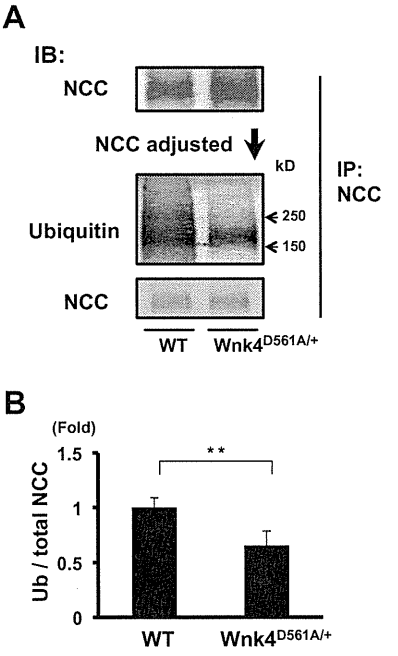

Fig. 2. Ubiquitination of NCC was reduced in *Wnk4*$^{D561A/+}$ mouse kidney. (A) Representing immunoblots of NCC ubiquitination in *Wnk4*$^{D561A/+}$ mouse kidney. NCC was immunoprecipitated from kidney homogenates of *Wnk4*$^{D561A/+}$ mice and their wild-type littermates. Immunoprecipitated NCC was adjusted to have nearly equal amounts of immunoprecipitated NCC in each lane in order to more clearly demonstrate the differences in ubiquitination in each lane. NCC ubiquitination was lower in *Wnk4*$^{D561A/+}$ mice, as compared to their wild-type littermates. (B) Densitometry analysis of NCC ubiquitination in *Wnk4*$^{D561A/+}$ mice. Ubiquitination of NCC in *Wnk4*$^{D561A/+}$ mice was significantly lower, as compared to their wild-type littermates. Values ($n = 5$) are normalized by immunoprecipitated total NCC. $^{**}P < 0.01$.

3.2. Decreased ubiquitination of NCC due to increased phosphorylation is involved in pathogenesis of PHAII

Previously, we generated *Wnk4*$^{D561A/+}$ knock-in mice, a mouse model of PHAII, and found that the pathogenesis of PHAII involves the constitutive activation of the WNK-OSR1/SPAK kinases-NCC phosphorylation cascade, resulting in the gain of NCC function. In this PHAII mouse model, both total and phosphorylated NCC was elevated in the kidney [3]. As observed in the mice fed low-salt diet, NCC was less ubiquitinated in the PHAII model mouse kidney, as compared with wild-type littermates (Fig. 2). These results clearly indicate that increased phosphorylation of NCC by activated WNK-OSR1/SPAK-NCC phosphorylation cascade results in decreased ubiquitination of NCC.

3.3. Phosphorylation of NCC decreased its ubiquitination

In mice, the major sites of NCC phosphorylation by OSR1 and SPAK are Thr 53, Thr 58 and Ser 71 [4]. To clarify the relationship between the phosphorylation of NCC at these sites and NCC ubiquitination, we transfected T7-tagged phospho-deficient and -mimicking mutant NCC along with wild-type NCC into COS7 cells (Fig. 3A), and evaluated the ubiquitination of these mutants. Immunoblots of whole cell lysates revealed that total protein abundance of the phospho-mimicking NCC was significantly higher than wild-type and phospho-deficient NCC, thus suggesting that degradation of the phospho-mimicking NCC is decreased (Fig. 3B and C). Ubiquitination of the phospho-mimicking NCC is less than that of wild-type and the phospho-deficient NCC, and is inversely correlated with total NCC abundance (Fig. 3D). These results clearly indicate that phosphorylation of NCC at Thr 53, Thr 58 and Ser 71 decreases NCC ubiquitination, and as a result, increases NCC protein abundance. It has been reported that NCC exhibits distinctive bands on immunoblots that correspond to molecular masses of 95, 110, 130 to 140 and more than 250 kDa [24,25]. Nonglycosylated 95 kDa NCC is the core NCC while the 110-kDa band is sensitive to Endo H digestion, corresponding to the endoplasmic reticulum- and/or pre-Golgi complex-retained NCC protein [24]. The glycosylated protein of 130–140 kDa is not sensitive to Endo H digestion and is present in the plasma membrane [24], forming functional homodimer complexes of 250–350 kDa [25]. In Fig. 3, the bands at 110, 130 and 250 kDa were all increased in the phospho-mimicking NCC, indicating that both NCC in the plasma membranes and in intracellular organelles is increased. We detected the smear-like ubiquitinated NCC band extending from about 120 to more than 250 kDa, thus suggesting that NCC ubiquitination in both ER/pre-Golgi and plasma membranes was decreased in the phospho-mimicking NCC.

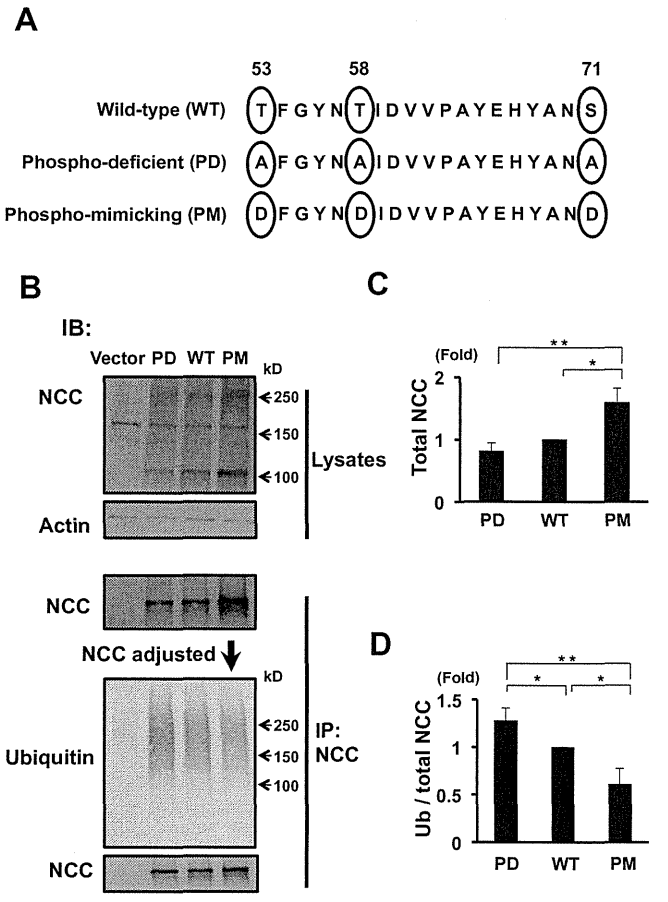

Fig. 3. NCC Phosphorylation increases total expression and decreases ubiquitination in COS7 cells. (A) Three consensus amino-terminal residues (T53, T58 and S71) are critical for the phosphorylation of NCC. In phospho-deficient NCC (PD), these residues are mutated to alanine. In phospho-mimicking NCC (PM), these residues are mutated to aspartic acid. (B) Representative immunoblots of expression and ubiquitination of phospho-deficient, wild-type or phospho-mimicking NCC. Empty vector (Vector), phospho-deficient, wild-type or phospho-mimicking T7-tagged NCC were transfected into COS7 cells. In total cell lysates, expression levels of phospho-mimicking NCC were higher than those of phospho-deficient and wild-type NCC (upper panel). NCC was immunoprecipitated from whole cell lysates, and immunoprecipitated NCC was adjusted to have nearly equal amounts of immunoprecipitated NCC in each lane in order to more clearly demonstrate the differences in ubiquitination in each lane (lower panels). Phospho-mimicking NCC is less ubiquitinated, as compared to phospho-deficient NCC. (C) Densitometry analysis of expression levels of phospho-deficient, wild-type and phospho-mimicking NCC in COS7 cells. Expression levels of phospho-mimicking NCC were significantly higher than those of phospho-deficient and wild-type NCC. For densitometry analysis, values ($n = 4$) are expressed as ratios against mean signals in wild-type NCC. $^{**}P < 0.01$, $^{*}P < 0.05$. (D) Densitometry analysis of ubiquitination of immunoprecipitated NCC from COS7 cells. NCC ubiquitination was corrected against NCC abundance. Phospho-mimicking NCC was significantly less ubiquitinated, as compared to wild-type and phospho-deficient NCC. Wild-type NCC was also less ubiquitinated than phospho-deficient NCC. For densitometry analysis, values ($n = 4$) are expressed as ratios against the mean signals in wild-type NCC. $^{**}P < 0.01$, $^{*}P < 0.05$.

3.4. Phosphorylation of NCC regulates its ubiquitination at the cell surface and increases membrane abundance

Ubiquitination is known to regulate cell surface abundance of ion channels and transporters [26]. Therefore, we examined the effects of NCC phosphorylation on the plasma membrane abundance of NCC, and also evaluated whether phosphorylation decreased NCC ubiquitination within the plasma membranes using the biotin–neutravidin system. Immunoblots of biotinylated cell surface protein with NCC antibody revealed that the cell surface expression of the phospho-mimicking NCC was much higher when compared with wild-type and phospho-deficient NCC (Fig. 4A and B). Biotinylated NCC exhibited bands at more than 250 kDa, indicating that our biotin assay detected NCC only in the plasma membranes. To evaluate the inhibitory effects of NCC phosphorylation on ubiquitination in plasma membranes, we isolated biotinylated surface NCC from COS7 cells by immunoprecipitation with NCC antibody, followed by NeutrAvidin pull down. As shown in Fig. 4C and D, the phospho-mimicking NCC in the plasma membranes showed less ubiquitination than wild-type and phospho-deficient NCC, indicating that the NCC phosphorylation decreases its ubiquitination within plasma membranes.

4. Discussion

The kidney plays an important role in linking salt intake with blood pressure. This vital function is regulated by sodium reabsorption through several ion-transporters expressed along the nephron. NCC plays a major role in renal electrolyte balance. Many

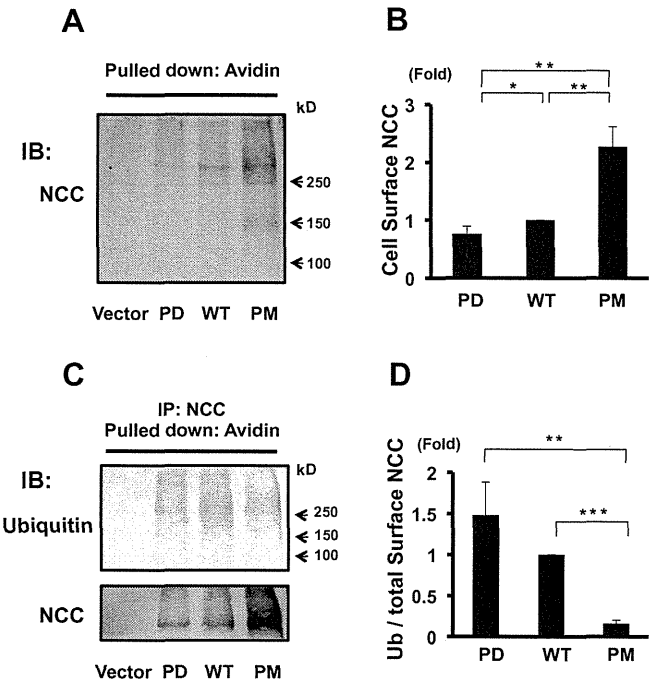

Fig. 4. NCC phosphorylation decreases its ubiquitination within plasma membranes. (A) Representative immunoblot of cell surface expression of phospho-deficient (PD), wild-type (WT) or phospho-mimicking (PM) NCC. COS7 cells were transfected with empty vector, PD, WT or PM T7-tagged NCC. Cell surface proteins were pulled down with biotinylation-neutravidin assay and blotted with anti-T7 antibody. (B) Densitometry analysis of surface NCC expression. Surface expression of phospho-mimicking NCC was also significantly higher than that of phospho-deficient and wild-type NCC. Surface expression of wild-type NCC was significantly higher than that of phospho-deficient NCC. For densitometry analysis, values are expressed as ratios against mean signals in wild-type NCC. $^{**}P < 0.01$, $^{*}P < 0.05$. (C) Representative blots of ubiquitination of biotinylated NCC. COS7 cells were transfected with empty vector, phospho-deficient (PD), wild-type (WT) or phospho-mimicking (PM) T7-tagged NCC. After cell surface biotinylation, NCC was immunoprecipitated by rabbit anti-NCC antibody. Immunoprecipitated and biotinylated NCC were pulled down with NeutrAvidin and blotted with ubiquitin and T7 antibody. In this experiment, immunoprecipitated-biotinylated NCC was not adjusted, as available samples in this assay were insufficient to be re-loaded. (D) Densitometry analysis of ubiquitination of immunoprecipitated NCC at the cell surface. Ubiquitination of phospho-mimicking NCC at the cell surface was much less than that of phospho-deficient and wild-type NCC. Ubiquitination of wild-type NCC was also less than that of phospho-deficient NCC, indicating that phosphorylation of NCC decreases its ubiquitination at the cell surface. For densitometry analysis, values ($n = 3$) are normalized against immunoprecipitated surface total NCC and are expressed as ratios against mean signals in wild-type NCC. $^{***}P < 0.001$ $^{**}P < 0.01$.

reports have shown that phosphorylation of NCC plays an essential role in NCC function [3–6,27,28]. In addition, total NCC abundance in the kidney appears to vary according to NCC phosphorylation status. However, it remains to be determined how the phosphorylation of NCC regulates its total protein abundance in the kidney. In this study, we clarified the role of phosphorylation on NCC abundance by focusing on NCC ubiquitination. We found that total protein abundance of the phospho-mimicking NCC in COS7 cells was significantly increased, as compared to phospho-deficient and wild-type NCC. Moreover, ubiquitination of phospho-mimicking NCC is lower than that of wild-type and phospho-deficient NCC, and inversely correlated with abundance (Fig. 3). These results clearly indicate that either phosphorylation of NCC inhibits or dephosphorylation of NCC promotes NCC ubiquitination, thereby regulating NCC abundance within cells.

This notion was supported by the *in vivo* evidence, i.e., the decreased NCC ubiquitination in *Wnk4*$^{D561A/+}$ knock-in PHAII model mice, where increased NCC phosphorylation and total protein abundance were observed in the kidney. As the mRNA of NCC was not increased in this PHAII mouse model (data not shown), it was clear that the degradation pathway of NCC played a key role in increased protein abundance. In addition to the PHAII mouse model, we also confirmed in wild-type mice that the increased and decreased phosphorylation of NCC by different salt diets decreased and increased NCC ubiquitination, respectively. Based on these data, we concluded that the ubiquitination of NCC is a major mechanism for regulating NCC protein abundance in kidney following changes in NCC phosphorylation.

In addition to total NCC protein abundance within cells, plasma membrane localization is important for NCC function *in vivo* [3]. Ubiquitination regulates a number of cell surface proteins by stimulating their internalization from the cell surface [26]. It was previously shown that NCC phosphorylated at Thr 53, Thr 58 and Ser 71 accumulated in the apical membranes of DCT, thus suggesting that phosphorylation of NCC is important for plasma membrane localization [7,8]. However, the underlying mechanism(s) remain to be determined. In our biotinylation assay, we demonstrated that phosphorylation of NCC regulates surface expression as observed in the *in vivo* kidney. Furthermore, we found that the phospho-mimicking NCC showed less ubiquitination within the plasma membranes (Fig. 4), thus suggesting that the phosphorylated NCC in the plasma membranes is less ubiquitinated, thereby increasing NCC abundance in plasma membranes. Although there have been several reports on the ubiquitination of NCC [18,19], further investigations will be required to clarify the detailed mechanism(s) of how phosphorylation of NCC affects the ubiquitination of NCC.

In summary, we demonstrated that NCC phosphorylation increased plasma membrane localization of NCC and decreased NCC ubiquitination. Decreased ubiquitination may be a major mechanism for accumulation of phosphorylated NCC in the plasma membranes.

Acknowledgments

This study was supported in part by Grants-in-Aid for Scientific Research (A) and for Scientific Research on Innovative Areas from the Japan Society for the Promotion of Science, Grant-in-Aid for Young Scientists (B) from the Ministry of Education, Culture, Sports, Science and Technology of Japan, Salt Science Research Foundation (No. 1228), Takeda Science Foundation, and The Nakajima Foundation.

References

[1] D.B. Simon, C. Nelson-Williams, M.J. Bia, D. Ellison, F.E. Karet, A.M. Molina, I. Vaara, F. Iwata, H.M. Cushner, M. Koolen, F.J. Gainza, H.J. Gitleman, R.P. Lifton, Gitelman's variant of Bartter's syndrome, inherited hypokalaemic alkalosis, is caused by mutations in the thiazide-sensitive Na–Cl cotransporter, Nat. Genet. 12 (1996) 24–30.

[2] F.H. Wilson, S. Disse-Nicodème, K.A. Choate, K. Ishikawa, C. Nelson-Williams, I. Desitter, M. Gunel, D.V. Milford, G.W. Lipkin, J.M. Achard, M.P. Feely, B. Dussol, Y. Berland, R.J. Unwin, H. Mayan, D.B. Simon, Z. Farfel, X. Jeunemaitre, R.P. Lifton, Human hypertension caused by mutations in WNK kinases, Science 293 (2001) 1107–1112.

[3] S.S. Yang, T. Morimoto, T. Rai, M. Chiga, E. Sohara, M. Ohno, K. Uchida, S.H. Lin, T. Moriguchi, H. Shibuya, Y. Kondo, S. Sasaki, S. Uchida, Molecular pathogenesis of *pseudohypoaldosteronism type II: generation and analysis of a* Wnk4(D561A/+) knockin mouse model, Cell Metab. 5 (2007) 331–344.

[4] C. Richardson, D.R. Alessi, The regulation of salt transport and blood pressure by the WNK-SPAK/OSR1 signalling pathway, J. Cell Sci. 121 (2008) 3293–3304.

[5] S.S. Yang, Y.F. Lo, C.C. Wu, S.W. Lin, C.J. Yeh, P. Chu, H.K. Sytwu, S. Uchida, S. Sasaki, S.H. Lin, SPAK-knockout mice manifest Gitelman syndrome and impaired vasoconstriction, J. Am. Soc. Nephrol. 21 (2010) 1868–1877.

[6] D. Pacheco-Alvarez, P.S. Cristóbal, P. Meade, E. Moreno, N. Vazquez, E. Muñoz, A. Díaz, M.E. Juárez, I. Giménez, G. Gamba, The Na^+:Cl^- cotransporter is activated and phosphorylated at the amino-terminal domain upon intracellular chloride depletion, J. Biol. Chem. 281 (2006) 28755–28763.

[7] N.B. Pedersen, M.V. Hofmeister, L.L. Rosenbaek, J. Nielsen, R.A. Fenton, Vasopressin induces phosphorylation of the thiazide-sensitive sodium *chloride cotransporter in the distal convoluted tubule*, Kidney Int. 78 (2010) 160–169.

[8] K. Mutig, T. Saritas, S. Uchida, T. Kahl, T. Borowski, A. Paliege, A. Böhlick, M. Bleich, Q. Shan, S. Bachmann, Short-term stimulation of the thiazide-sensitive Na^+–Cl^- cotransporter by vasopressin involves phosphorylation and membrane translocation, Am. J. Physiol. Renal Physiol. 298 (2010) F502–509.

[9] M. Chiga, T. Rai, S.S. Yang, A. Ohta, T. Takizawa, S. Sasaki, S. Uchida, Dietary salt regulates the phosphorylation of OSR1/SPAK kinases and the sodium chloride cotransporter through aldosterone, Kidney Int. 74 (2008) 1403–1409.

[10] G. Talati, A. Ohta, T. Rai, E. Sohara, S. Naito, A. Vandewalle, S. Sasaki, S. Uchida, Effect of angiotensin II on the WNK-OSR1/SPAK-NCC phosphorylation cascade in cultured mpkDCT cells and in vivo mouse kidney, Biochem. Biophys. Res. Commun. 393 (2010) 844–848.

[11] M.B. Sandberg, A.D. Riquier, K. Pihakaski-Maunsbach, A.A. McDonough, A.B. Maunsbach, ANG II provokes acute trafficking of distal tubule Na^+–Cl(–) cotransporter to apical membrane, Am. J. Physiol. Renal Physiol. 293 (2007) F662–669.

[12] P. San-Cristobal, D. Pacheco-Alvarez, C. Richardson, A.M. Ring, N. Vazquez, F.H. Rafiqi, D. Chari, K.T. Kahle, Q. Leng, N.A. Bobadilla, S.C. Hebert, D.R. Alessi, R.P. Lifton, G. Gamba, Angiotensin II signaling increases activity of the renal Na–Cl cotransporter through a WNK4-SPAK-dependent pathway, Proc. Natl. Acad. Sci. USA 106 (2009) 4384–4389.

[13] E. Sohara, T. Rai, S.S. Yang, A. Ohta, S. Naito, M. Chiga, N. Nomura, S.H. Lin, A. Vandewalle, E. Ohta, S. Sasaki, S. Uchida, Acute insulin stimulation induces phosphorylation of the Na–Cl cotransporter in cultured distal mpkDCT cells and mouse kidney, PLoS One 6 (2011) e24277.

[14] F.H. Rafiqi, A.M. Zuber, M. Glover, C. Richardson, S. Fleming, S. Jovanović, A. Jovanović, K.M. O'Shaughnessy, D.R. Alessi, Role of the WNK-activated SPAK kinase in regulating blood pressure, EMBO Mol. Med. 2 (2010) 63–75.

[15] R. Zhou, S.V. Patel, P.M. Snyder, Nedd4-2 catalyzes ubiquitination and degradation of cell surface ENaC, J. Biol. Chem. 282 (2007) 20207–20212.

[16] L. Schild, Y. Lu, I. Gautschi, E. Schneeberger, R.P. Lifton, B.C. Rossier, Identification of a PY motif in the epithelial Na channel subunits as a target sequence for mutations causing channel activation found in Liddle syndrome, EMBO J. 15 (1996) 2381–2387.

[17] K.K. Knight, D.R. Olson, R. Zhou, P.M. Snyder, Liddle's syndrome mutations increase Na^+ transport through dual effects on epithelial Na^+ channel surface expression and proteolytic cleavage, Proc. Natl. Acad. Sci. USA 103 (2006) 2805–2808.

[18] P.G. Needham, K. Mikoluk, P. Dhakarwal, S. Khadem, A.C. Snyder, A.R. Subramanya, J.L. Brodsky, The thiazide-sensitive NaCl cotransporter is targeted for chaperone-dependent endoplasmic reticulum-associated degradation, J. Biol. Chem. 286 (2011) 43611–43621.

[19] J.P. Arroyo, D. Lagnaz, C. Ronzaud, N. Vázquez, B.S. Ko, L. Moddes, D. Ruffieux-Daidié, P. Hausel, R. Koesters, B. Yang, J.B. Stokes, R.S. Hoover, G. Gamba, O. Staub, Nedd4-2 modulates renal Na^+–Cl^- cotransporter via the aldosterone-SGK1-Nedd4-2 pathway, J. Am. Soc. Nephrol. 22 (2011) 1707–1719.

[20] T. Moriguchi, S. Urushiyama, N. Hisamoto, S. Iemura, S. Uchida, T. Natsume, K. Matsumoto, H. Shibuya, WNK1 regulates phosphorylation of cation-chloride-coupled cotransporters via the STE20-related kinases, SPAK and OSR1, J. Biol. Chem. 280 (2005) 42685–42693.

[21] K. Susa, S. Kita, T. Iwamoto, S.S. Yang, S.H. Lin, A. Ohta, E. Sohara, T. Rai, S. Sasaki, D.R. Alessi, S. Uchida, *Effect of heterozygous deletion of WNK1 on the* WNK-OSR1/SPAK-NCC/NKCC1/NKCC2 signal cascade in the kidney and blood vessels, Clin. Exp. Nephrol. (2012).

[22] K. Oi, E. Sohara, T. Rai, M. Misawa, M. Chiga, D.R. Alessi, S. Sasaki, S. Uchida, A minor role of WNK3 in regulating phosphorylation of renal NKCC2 and NCC co-transporters in vivo, Biol. Open 1 (2011) 120–127.

[23] A. Ohta, T. Rai, N. Yui, M. Chiga, S.S. Yang, S.H. Lin, E. Sohara, S. Sasaki, S. Uchida, Targeted disruption of the Wnk4 gene decreases phosphorylation of Na–Cl cotransporter, increases Na excretion and lowers blood pressure, Hum. Mol. Genet. 18 (2009) 3978–3986.

[24] J.C. De Jong, W.A. Van Der Vliet, L.P. Van Den Heuvel, P.H. Willems, N.V. Knoers, R.J. Bindels, Functional expression of mutations in the human NaCl cotransporter: evidence for impaired routing mechanisms in Gitelman's syndrome, J. Am. Soc. Nephrol. 13 (2002) 1442–1448.
[25] J.C. de Jong, P.H. Willems, F.J. Mooren, L.P. van den Heuvel, N.V. Knoers, R.J. Bindels, The structural unit of the thiazide-sensitive NaCl cotransporter is a homodimer, J. Biol. Chem. 278 (2003) 24302–24307.
[26] L. Hicke, R. Dunn, Regulation of membrane protein transport by ubiquitin and ubiquitin-binding proteins, Annu. Rev. Cell Dev. Biol. 19 (2003) 141–172.
[27] S. Uchida, Pathophysiological roles of WNK kinases in the kidney, Pflugers Arch. 460 (2010) 695–702.
[28] J.A. McCormick, J.H. Nelson, C.L. Yang, J.N. Curry, D.H. Ellison, Overexpression of the sodium chloride cotransporter is not sufficient to cause familial hyperkalemic hypertension, Hypertension 58 (2011) 888–894.

Original Paper

Cellular Physiology and Biochemistry

Cell Physiol Biochem 2012;29:65-74

Accepted: December 16, 2011

A New Role for Aquaporin 7 in Insulin Secretion

Karim Louchami[1], Len Best[2], Peter Brown[2], Myrna Virreira[3], Emeline Hupkens[1], Jason Perret[4], Olivier Devuyst[5], Shinichi Uchida[6], Christine Delporte[4], Willy J. Malaisse[1], Renaud Beauwens[3] and Abdullah Sener[1]

[1]Laboratory of Experimental Hormonology, Université Libre de Bruxelles, Brussels, [2]Schools of Medicine and Life Sciences, University of Manchester, Manchester, [3]Laboratory of Cell and Molecular Physiology, Université Libre de Bruxelles, Brussels, [4]Laboratory of Biological Chemistry and Nutrition, Université Libre de Bruxelles, Brussels, [5]Division of Nephrology, Université Catholique de Louvain, Brussels, Belgium and [6]Department of Nephrology, Graduate School of Medicine, Tokyo Medical and Dental University, Tokyo

Key Words

AQP7 • Insulin-producing β-cells • Insulin secretion • Cell swelling

Abstract

Bacgrouns/Aims: Several insulinotropic agents were recently reported to cause β-cell swelling. The possible participation of AQP7 to water transport was investigated in AQP7$^{+/+}$ or AQP7$^{-/-}$ mice. Methods: Aquaporin expression, insulin secretion, cell swelling and electrical activity were investigated in pancreatic islets. Results: RT-PCR revealed the expression of AQP5 and AQP8 mRNA. Double immunofluorescent labeling indicated their presence in β-cells. Whilst basal insulin release from isolated pancreatic islets incubated at 2.8 mM D-glucose did not differ between AQP7$^{+/+}$ or AQP7$^{-/-}$ mice, the secretion of insulin evoked by the omission of 50 mM NaCl, the substitution of 50 mM NaCl by 100 mM glycerol or a rise in D-glucose concentration to 8.3 mM and 16.7 mM was severely impaired in the islets from AQP7$^{-/-}$ mice. Yet, exposure of β-cells to either the hypotonic medium or a rise in D-glucose concentration caused a similar degree of swelling and comparable pattern of electrical activity in cells from AQP7$^{+/+}$ and AQP7$^{-/-}$ mice. Both the cell swelling and change in membrane potential were only impaired in AQP7$^{-/-}$ cells when exposed to 50 mM glycerol. Conclusion: It is proposed, therefore, that AQP7 may, directly or indirectly, play a role at a distal site in the exocytotic pathway.

Introduction

Aquaporins are channel-forming membrane proteins which allow water movement through the plasma membrane [1]. Aquaglyceroporins represent a subfamily of aquaporins permeable not only to water but also to small solutes like glycerol and urea [1, 2]. Aquaglyceroporin 7 (AQP7) is expressed in rat and mouse pancreatic islet β-cells and tumoral insulin-producing BRIN-BD11 cells [3-5]. Matsumura et al. [5] first reported that islets isolated from AQP7$^{-/-}$ mice secrete more insulin than islets obtained from AQP7$^{+/+}$ mice, when incubated at either low (5.6 mM) or high (25.0 mM) D-glucose concentration, despite a lower islet insulin content in the former AQP7$^{-/-}$ mice than in the latter AQP7$^{+/+}$ mice. Incidentally and quite surprisingly, assuming an islet protein content close to 1.0 μg/islet [6], the secretion of

KARGER

Fax +41 61 306 12 34
E-Mail karger@karger.ch
www.karger.com

1015-8987/12/0292-0065$38.00/0

Accessible online at:
www.karger.com/cpb

A. Sener
Laboratory of Experimental Hormonology, Université Libre de Bruxelles
808 Route de Lennik, B-1070 Brussels (Belgium)
Tel. +32-2-555 62 40, Fax +32-2-555 42 19
E-Mail abdsener@ulb.ac.be

insulin by islets from AQP7$^{+/+}$ mice recorded in the presence of 25.0 mM D-glucose was about two orders of magnitude lower (ca. 23.8 ± 1.5 pg/μg protein per hour; n = 3) in the study by Matsumura et al. [5] than that found either by Li et al. [7] in islets from wild-type mice incubated in the presence of 20.0 mM D-glucose (about 2.0 ± 0.1 ng/μg protein per hour; n = 9-23) or by Bulur et al. [8] in islets from NMRI mice incubated at 16.7 mM D-glucose (3.8 ± 0.5 ng/μg protein per hour). An even more pronounced relative difference (about 400-fold) prevails when comparing the insulin content from wild-type mice in the report by Matsumura et al. (113.4 ± 7.2 pg/μg protein; n = 8) and either Li et al. (47 ± 3 ng/μg protein; n = 6-8) or Bulur et al. (46 ± 1 ng/μg protein; n = 88). Matsumura et al. [5] also observed increased intraislet glycerol and triglyceride contents in the AQP7$^{-/-}$ mice compared to those in the AQP7$^{+/+}$ mice. They concluded that AQP7 appears to be a key regulator of intracellular glycerol content as well as insulin production and secretion.

Another possible role for aquaporins in the process of nutrient-stimulated insulin secretion is currently considered in the framework of the so-called volume-regulated anion channel hypothesis [9, 10]. It postulates that, in addition to metabolically-regulated K_{ATP} channels, β-cells are equipped with volume-regulated anion channels (VRAC) that are activated by D-glucose concentrations within the range effective in modulating electrical activity and insulin release. More precisely, it is proposed that the intracellular accumulation of lactate and bicarbonate anions generated in insulin-producing cells by the catabolism of D-glucose leads to cell swelling and, hence, gating of the volume-sensitive anion channels, eventually leading to plasma membrane depolarization and subsequent gating of voltage-dependent calcium channels [11]. Such a hypothesis motivated recent investigations in the perspective of the possible participation of AQP7 to the regulation of insulin secretion in pancreatic β-cells. For instance, it was recently demonstrated that glycerol depolarizes pancreatic β-cells, resulting in electrical and secretory activity [3]. Similar effects were observed using a non-metabolizable glycerol analogue, 1,3-propanediol, and with urea. In common with glycerol, these osmolytes permeate the β-cell plasma membrane, probably via AQP7. In fair agreement with the latter proposal, the net uptake of [2-^{3}H]glycerol by BRIN-BD11 cells increased to 143 ± 4% of its control value within 2 min incubation in a hypotonic extracellular medium and progressively declined thereafter, both the relative magnitude and time course of such changes being similar to those observed under the same experimental conditions for the initial increase in cell volume and later regulatory volume decrease [4,12].

Gene	Sequence of primers	Amplicons (bp)
AQP5	Forward: TGGAGCAGGCATCCTGTACT Reverse: CGTGGAGGAGAAGATGCAGA	111
AQP7	Forward: CGTGGCTCACATGGTTTTAG Reverse: AGAGATGCCGCCTGCTAC	106
AQP8	Forward: ATGGCTGGCTACTGGGACTT Reverse: CGCCAGCAGTTCTTCTTCAC	105

Table 1. Sequences of forward and reverse primers used for RT-PCR amplification.

Based on a comparison between AQP7$^{+/+}$ wild-type mice and AQP7$^{-/-}$ knockout mice, this study further investigates the role of AQP7 in pancreatic β-cell function. Taking also into account novel information on the expression of AQP5 and AQP8 in insulin-producing cells, the present report proposes a new role for AQP7 in insulin secretion.

Materials and Methods

Animals

AQP7$^{-/-}$ mice were generated at Tokyo Medical and Dental University by targeted deletion of exon 2 [13] and sent to Belgium, where they were maintained in air-filtered cages and fed normal mouse chow in the Division of Nephrology of the Université Catholique de Louvain. Body weight, as well as plasma D-glucose [14] and insulin [15] concentration were measured in male and female AQP7$^{+/+}$ and AQP7$^{-/-}$ mice by methods described in the cited references.

Islet isolation

Pancreatic islets were isolated by the collagenase procedure [16].

RT-PCR

Total RNA from mouse tissues was extracted using the AURUM™ total RNA fatty acid and tissue kit (BioRad, Hercules, CA, USA). The purified total RNA was quantified on a Nanodrop spectrophotometer (NanoDrop Technologies, Inc, Wilmington, DE, USA). Quality of the total RNA was verified on an Experion Automated Electrophoresis System (BioRad, Hercules, CA, USA). The total RNA was reverse transcribed using the Revert Aid™ first strand cDNA synthesis kit (Fermentas, St. Leon-Rot, Germany), starting from 1 μg total RNA in a final 20 μl reaction volume. The sequences of forward and reverse mouse AQPs and beta actin are shown in Table 1. All PCR reactions were performed in a total volume of 20 μl containing 1 μl of cDNA, 0.5 U GoTaq DNA polymerase (Promega, Madison, WI, USA), 0.2 mM dNTP, 0.5 μM of each primer, and 4 μl GoTaq Green 5x buffer using My iCycler Thermal

cycler (Bio-Rad Laboratories, Hercules, USA). Thermocycling conditions were 94°C for 1.5 min followed by 35 cycles of 30 sec at 95°C, 30 sec at 60°C and 1 min at 72°C. The PCR amplification products were submitted to electrophoresis on a 1.2% agarose gel in TAE buffer: 40 mM Tris, 40 mM Acetate, 1 mM EDTA in the presence of 0.5 μg/ml of ethidium bromide. Gels were visualized by UV translumination using a GelDoc apparatus (Bio-Rad Laboratories, Hercules, USA).

Double fluorescence immunolabelling

Several sections of mouse pancreas, embedded in paraffin (4 μm thickness), were deparaffined, rehydrated and then incubated overnight at 4°C with primary antibodies as follows: rabbit polyclonal affinity purified anti-AQP5 (Millipore, Billerica, MA, USA) or anti-AQP8 (Alpha Diagnostics, San Antonio, TX, USA) at dilution 1:100 and mouse monoclonal affinity-purified anti-insulin at dilution 1:100 (Abcam, Cambridge, United Kingdom). Bound antibodies were revealed by incubating the tissue slices with anti-rabbit biotin antibodies at a dilution of 1:200 in PBS containing 5% horse serum (GE Healthcare, Little Chalfont, United Kingdom) for 120 min. This was followed by incubation with streptavidin-Cyanin2 (dilution 1:300 in PBS containing 5% horse serum (GE Healthcare, Little Chalfont, United Kingdom)) and anti-mouse-Cyanin3 (dilution 1:300 in PBS containing 5% horse serum (GE Healthcare, Little Chalfont, United Kingdom) for 120 min. Slides were mounted using Pro-Long Gold antifade reagent (Invitrogen, Eugene, USA). As negative controls, tissue sections were incubated either with secondary antibody alone, or with anti-AQP antibody pre-adsorbed with a 100-fold excess of the immunizing peptide. Images were taken using an Axiocam MRB fluorescent microscope using a 40x objective.

Insulin secretion

Insulin secretion was measured in groups of 8 islets incubated for two successive periods of 30 min each in 1.0 ml of salt-balanced medium [16] containing 5.0 mg/ml bovine albumin and equilibrated against a mixture of O_2-CO_2 (95-5, v-v).

Cell volume and electrical activity

Cell volume measurements and electrophysiological recordings were carried out on isolated mouse β-cells. For this purpose, islets were dispersed by brief exposure to Ca^{2+}-free medium containing NaCl (130 mM), KCl (5 mM), $MgCl_2$ (1 mM), D-glucose (5 mM) EGTA (1 mM) and HEPES-NaOH (20 mM; pH 7.4). Islet cells were centrifuged at 500g for 5 min, re-suspended in HEPES-buffered Minimal Essential Medium (Invitrogen, Paisley, UK) supplemented with 5% (v/v) foetal calf serum and 50 μg/ml gentamicin and cultured in 30 mm diameter polystyrene dishes for up to one week in humidified air at 37°C. Relative cell volume (RCV) was measured using a video-imaging technique as described previously [3, 17]. β-cells were distinguished from other islet cells by size and characteristic granular appearance. The mean volume (± SEM) of the cells used in this study was 3.3 ± 0.2 pl (n = 45; range 1.7 to 5.7 pl). Two series of experiments were performed. In the first the effects of superfusing cells with a hypotonic solution were examined. The isotonic solution (329 ± 1 mOsmol.Kg H_2O^{-1}, n = 6) contained NaCl (139 mM), KCl (5 mM), $NaHCO_3$ (25 mM), D-glucose (2.8 mM), mannitol (13.9 mM), $MgCl_2$ (1.2 mM), $CaCl_2$ (1 mM) with a pH 7.4 and was gassed with 95% O_2 and 5% CO_2. The hypotonic solution (236 ± 1 mOsmol.Kg H_2O^{-1}, n = 5) had a similar composition but contained only 89 mM NaCl and no mannitol. The second series of experiments examined volume changes in response to solutions containing either an increased glucose concentration or glycerol. The solutions used in these experiments were similar to those employed in previous studies examining the effects of D-glucose [17] and glycerol [3] on cell volume. Thus, in the D-glucose experiments the solutions (pH 7.4) contained NaCl (110 mM), KCl (5 mM), $NaHCO_3$ (25 mM), $MgCl_2$ (1.2 mM), $CaCl_2$ (1 mM) and were gassed with 95% O_2 and 5% CO_2. The D-glucose concentrations were either 4 or 20 mM and osmolality was maintained at 290 ± 2 mOsmol.Kg H_2O^{-1}, n = 3) by the addition of 16 mM mannitol to the 4 mM D-glucose solution. Hepes-buffered solutions were used in the glycerol experiments, and these contained NaCl (120 mM), KCl (5 mM), D-glucose (4 mM), $MgCl_2$ (1.2 mM), $CaCl_2$ (1 mM), Hepes/NaOH (5 mM; pH 7.4) and either 50 mM mannitol (309 ± 0 mOsmol.Kg H_2O^{-1}, n = 3) or 50 mM glycerol (307 ± 1 mOsmol.Kg H_2O^{-1}, n = 3). Cells were superfused with these solutions at a rate of 5.5 ml.min^{-1} and at a temperature of 37°C. Images were saved as JPEG files at a rate of 1 per minute, except in one series of experiments in which the rate of cell swelling in the hypotonic solution was recorded at one image every 15 seconds. Cell volume was calculated from the area of each image assuming the cells are spherical. Volumes were normalised to the volume observed during the 2 min control period at the beginning of each experiment (relative cell volume). Cells were equilibrated with the experimental solution for 8 min before each experiment. Rates of volume change were calculated by linear regression analysis of the linear phase (a minimum of 4 data points were employed in these calculations). Volume changes in response to glucose and glycerol were calculated using the area under the curve function of Graphpad 5 (Prism software).

β-cell electrical activity

The electrical activity of β-cells was recorded by means of the perforated patch technique using a List EPC-7 amplifier in current clamp mode as described previously [18]. Cells were superfused with a bath solution consisting of NaCl (130 mM), KCl (4 mM), $MgCl_2$ (1.2 mM), $CaCl_2$ (1 mM), D-glucose (2.8 mM) and HEPES-NaOH (20 mM; pH 7.4). For experiments studying the effects of glycerol, the basal medium contained 50 mM mannitol substituted for 25 mM NaCl. The addition of glycerol to the medium was then substituted for an eqivalent amount of mannitol. The pipette solution contained KCl (130 mM), NaCl (4 mM), $MgCl_2$ (1 mM), HEPES-NaOH (10 mM; pH 7.2) and gramicidin D (50 μg/ml) as perforating agent. Activity of the volume-regulated anion channel (VRAC) was measured using the conventional whole-cell recording technique [19]. Cell swelling was induced by use of a hypertonic pipette solution consisting of CsCl (60 mM), $MgCl_2$ (2 mM), ATP (1 mM), EGTA (1 mM), mannitol (220 mM) and HEPES (10 mM, pH 7.2). CsCl (1 mM) was added to the bath solution to block inward K^+ currents. Cells were held at 0 mV and subjected to 50 msec voltage pulses

Mice	Body weight (g)	Plasma D-glucose (mM)	Plasma insulin (μU/ml)
Male AQP7$^{+/+}$	26.3 ± 1.4 (10)	5.91 ± 0.92 (7)	9.4 ± 1.9 (6)
Female AQP7$^{+/+}$	22.9 ± 0.6 (11)	5.74 ± 0.75 (7)	8.9 ± 2.8 (6)
Male AQP7$^{-/-}$	26.1 ± 1.4 (10)	6.38 ± 1.16 (7)	8.1 ± 1.5 (6)
Female AQP7$^{-/-}$	23.1 ± 0.6 (15)	5.53 ± 0.65 (10)	6.6 ± 1.3 (9)

Table 2. Body weight, plasma D-glucose and insulin concentrations.

of ± 100 mV at 2 sec intervals. Cell capacitance (7-11 pF) was measured by nulling the capacitance transients, and current density expressed as pA/pF.

Statistical analysis

All results are expressed as means ± SEM. The statistical significance of differences between mean values was assessed by use of Student's *t*-test.

Results

Body weight, plasma D-glucose and insulin concentrations

As shown in Table 2, both the AQP7$^{+/+}$ and AQP7$^{-/-}$ female mice displayed a lower body weight ($p < 0.05$ or less) than the corresponding male mice. No significant difference was observed between the four groups of mice listed in Table 2, in terms of either plasma D-glucose or insulin concentration.

Aquaporin expression in rat pancreatic islet cells

Screening of AQP5 mRNA expression in mouse pancreatic islet cells was performed by RT-PCR, using β-actin primers or mouse AQP5 specific primers on cDNA obtained from purified total RNA isolated from several mouse tissues (used as positive controls) and mouse pancreatic islet cells. The amplification reaction yielded single amplicon of the expected molecular weight for β-actin, AQP5 and AQP8 in pancreatic islet cells from both AQP7$^{+/+}$ and AQP7$^{-/-}$ mice (Fig. 1), whilst such was only the case for AQP7 in islet cells from AQP7$^{+/+}$ mice as distinct from AQP7$^{-/-}$ mice.

Double immunofluorescence labeling of AQPs and insulin in mouse pancreatic sections indicated that AQP5 and AQP8 were expressed by insulin-producing β-cells (Fig. 2).

Insulin secretion

In a first series of experiments, the release of insulin over 30 min preincubation in an isotonic medium containing 2.8 mM D-glucose did not differ significantly ($p > 0.5$) from the islets of either AQP7$^{+/+}$ mice (12.0 ± 1.1 μU/islet; n = 60) or AQP7$^{-/-}$ mice (13.0 ± 1.3 μU/islet; n = 60). When further incubated for 30 min under the same experimental conditions, the release of insulin, expressed relative to the paired value recorded during preincubation, again failed to differ significantly ($p = 0.95$) in the WT animals (50.7 ± 4.7%; n = 20) and knock-out mice (50.1 ± 8.3%; n = 20). When the final incubation was conducted at the low D-glucose concentration (2.8 mM) in a medium of low osmolarity, as provoked by the omission of 50 mM NaCl, the paired incubation/preincubation ratio for insulin release averaged, in the control animals, 204.8 ± 54.2% (n = 20), a value 4-fold higher ($p < 0.008$) than that recorded when both the preincubation and incubation were conducted in an isotonic medium (Fig. 3). In the knockout mice, however, the paired incubation/preincubation ratio after exposure to the hypotonic medium did not exceed (61.6 ± 6.6%; n = 18), a value no more significantly different ($p > 0.29$) from

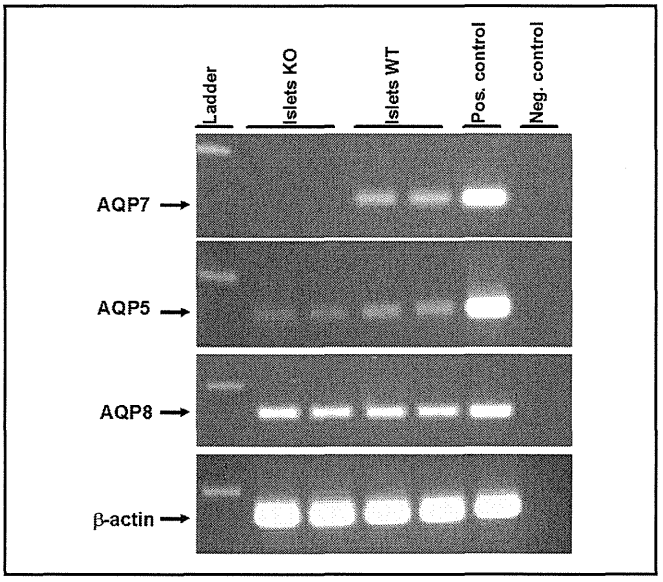

Fig. 1. RT-PCR detection of AQP7, AQP5 and AQP8 mRNA: PCR amplicons using AQP7, AQP5 and AQP8 primers from mouse WT and KO pancreatic islets. Kidney, lung and liver served as positive control for AQP7, AQP5 and AQP8 respectively. Negative control: absence of target. Ladder: 1Kb molecular weight marker. β-actin: served to test the integrity of extracted cDNA.

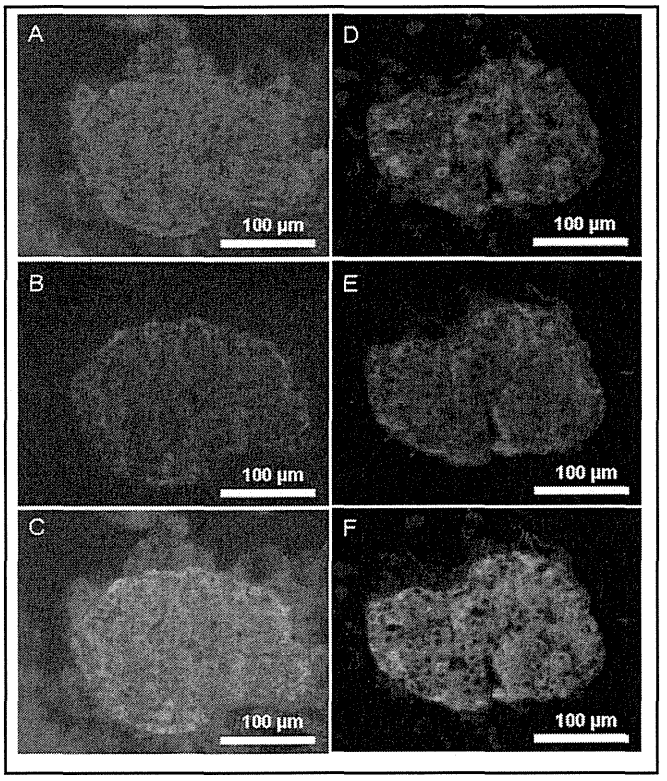

Fig. 2. Immolabelling of AQP5 and AQP8 proteins in mouse pancreatic β-cells. A, B and C: double fluorescence labelling for AQP8 and insulin; D, E and F: double fluorescence labelling for AQP5 and insulin. A and D: AQP labelling (in green); B and E: insulin labelling (in red); C and F: overlapping of AQP and insulin labelling (in orange). Scale bar represents 100 µm.

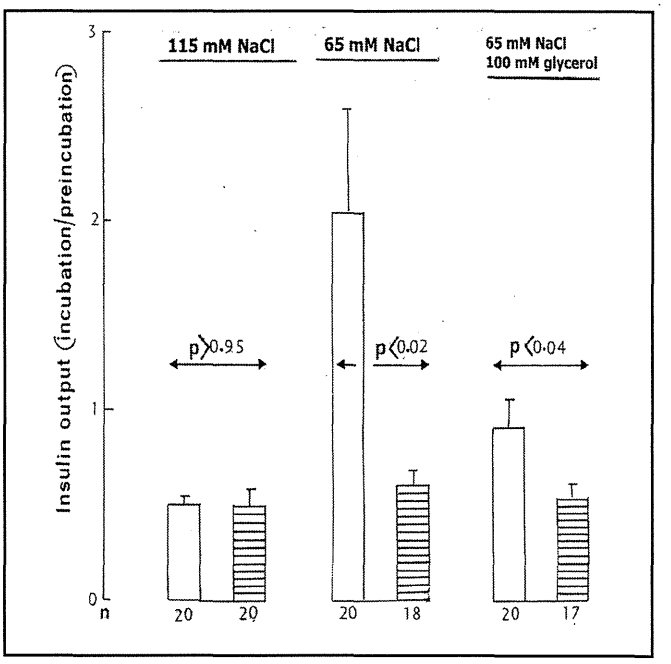

Fig. 3. Paired incubation/preincubation ratio for insulin output by islets prepared from either AQP7$^{+/+}$ mice (open columns) or AQP7$^{-/-}$ (hatched column), preincubated for 30 min in an isotonic medium containing 2.8 mM D-glucose, and then incubated at the same hexose concentration in either an isotonic salt-balanced medium containing 115 mM NaCl (left), a hypotonic medium only containing 65 mM NaCl (middle) or the same medium enriched with 100 mM glycerol (right). Mean values (± SEM) refer to the number of individual determinations indicated below each column, and are shown together with the statistical significance of differences between control animals and knock-out mice.

Fig. 4. Paired incubation/preincubation ratio for insulin output by islets prepared from either AQP7$^{+/+}$ mice (open columns) or AQP7$^{-/-}$ mice (hatched columns), preincubated for 30 min in an isotonic medium containing 2.8 mM D-glucose, and then incubated either at the same hexose concentration in the same isotonic medium (left), or in the same medium containing 8.3 mM (middle) or 16.7 mM (right) D-glucose. Mean values (± SEM) refer to the number of individual observations indicated below each column, and are shown together with the statistical significance of differences between control animals and knock-out mice.

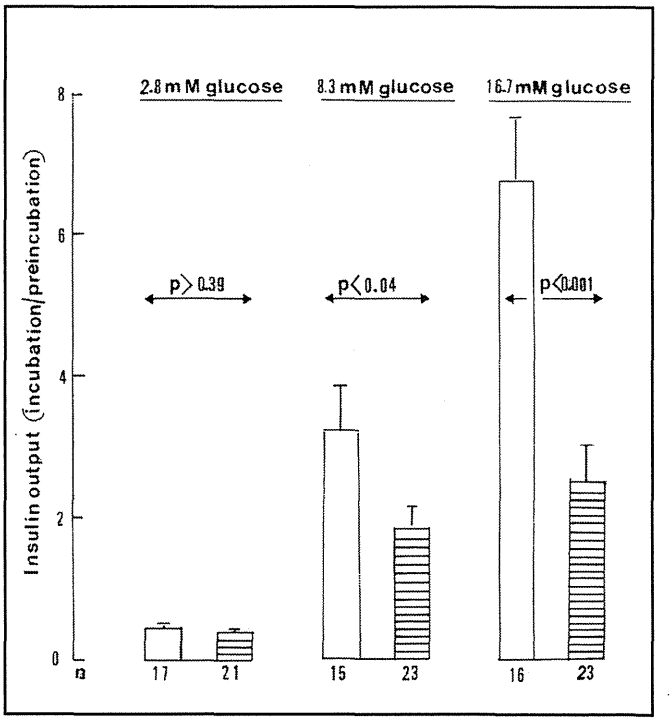

that recorded, in the same mice, when both the preincubation and incubation were conducted in an isotonic medium. When the final incubation medium was conducted in an isotonic medium, in which 50 mM NaCl was substituted by 100 mM glycerol, the incubation/preincubation ratio for insulin release averaged, in the control animals, 91.6 ± 13.9% (n = 20) a value again significantly higher ($p < 0.009$) from that recorded when both the preincubation and incubation were conducted in an isotonic medium. In the knock-out mice, the incubation/

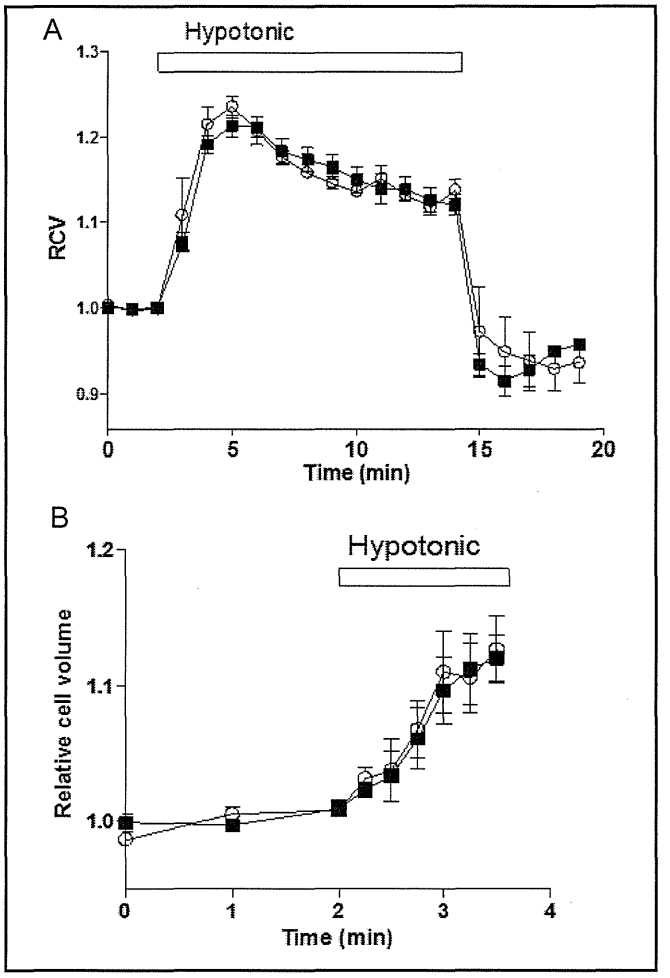

Fig. 5. (A) Effects of a 33% decrease in extracellular osmolarity on the relative cell volume (RCV) of mouse pancreatic β-cells from AQP7$^{+/+}$ (closed squares; n = 7) or AQP7$^{-/-}$ (open circles; n = 4) mice. (B) The lower panel illustrates the early changes in cell volume during the first 90 seconds of exposure to the hypotonic medium in cells from AQP7$^{+/+}$ (closed squares; n =6) or AQP7$^{-/-}$ (open circles; n = 6) mice. Data are mean values (± SEM).

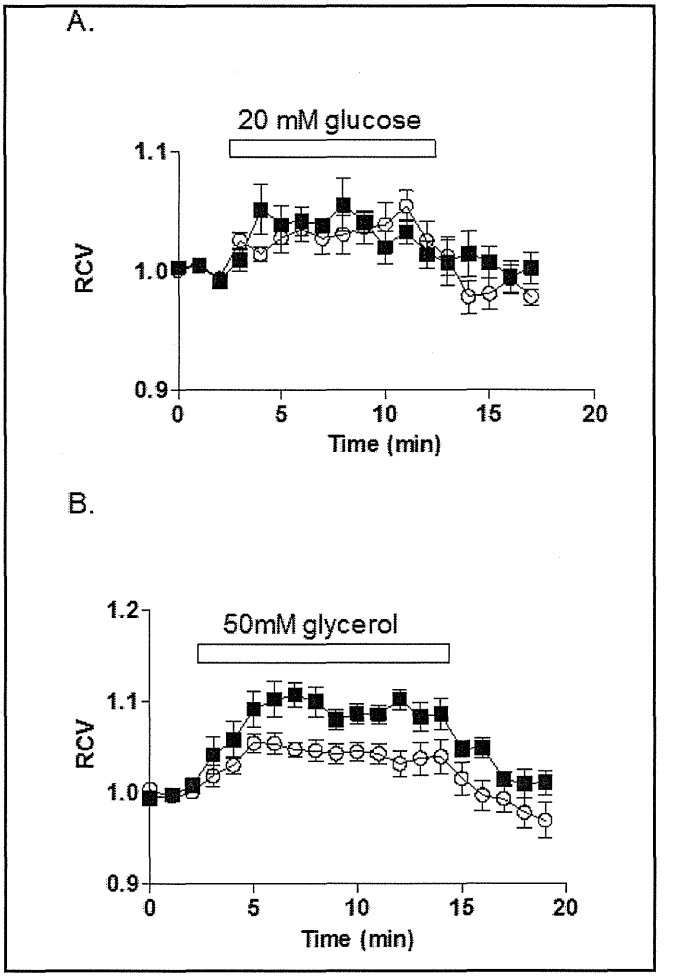

Fig. 6. (A) Effects of a rise in D-glucose concentration from 4 to 20 mM (associated with a decrease in mannitol concentration from 16 to zero mM, in order to maintain isotonicity) on the relative cell volume (RCV) of mouse pancreatic β-cells from AQP7$^{+/+}$ (closed squares) and AQP7$^{-/-}$ (open circles) mice. Mean values (± SEM) refer to 6 individual experiments. (B) Effects of the substitution of 50 mM mannitol by 50 mM glycerol on the relative cell volume of β-cells from AQP7$^{+/+}$ (closed squares) and AQP7$^{-/-}$ (open circles) mice. Mean values (± SEM) refer to 6 individual experiments.

preincubation ratio for insulin output after exposure to the isotonic medium with substitution of NaCl (50 mM) by glycerol (100 mM) did not exceed 54.7 ± 7.7% n = 17) and, as such, failed to differ significantly ($p > 0.69$) from that recorded in the same mice when both the preincubation and incubation were conducted in the control isotonic medium.

In a second series of experiments, the islets from control and knock-out mice were again preincubated for 30 min in a salt-balanced medium containing 2.8 mM D-glucose and then incubated in the same medium containing either 2.8, 8.3 or 16.7 mM D-glucose (Fig. 4). During the preincubation, the release of insulin was not significantly different ($p > 0.18$) in the islets from control mice (24.0 ± 2.9 μU/islet; n = 52) and knock-out mice (19.9 ± 1.6 μU/islet; n = 71). When the islets were further incubated at 2.8 mM D-glucose, the release of insulin expressed relative to the paired value recorded during preincubation also failed to differ significantly ($p > 0.39$) in the control mice (44.8 ± 5.7%; n = 17) and knock-out mice (38.3 ± 5.1%; n = 21). However, when the islets were eventually incubated at 8.3 mM D-glucose, the paired incubation/preincubation ratio for insulin output was lower ($p < 0.04$) in the knock-out mice (185.5 ± 29.6%; n = 23) than in the control mice (323.9 ± 64.2%; n = 15). The latter two percentages were both much higher ($p < 0.001$) than those

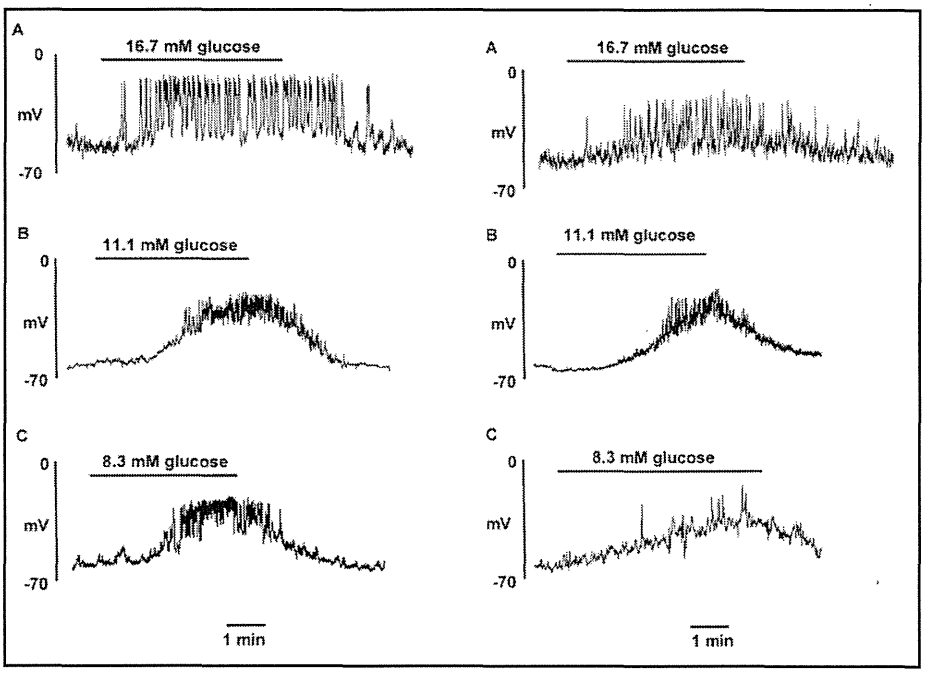

Fig. 7. Effects of a rise in D-glucose concentration from 2.8 to 8.3, 11.1 or 16.7 mM on membrane potential in AQP7$^{+/+}$ (left panel) or AQP7$^{-/-}$ (right panel) mouse pancreatic β-cells. Recording are representative of 3 - 5 cells.

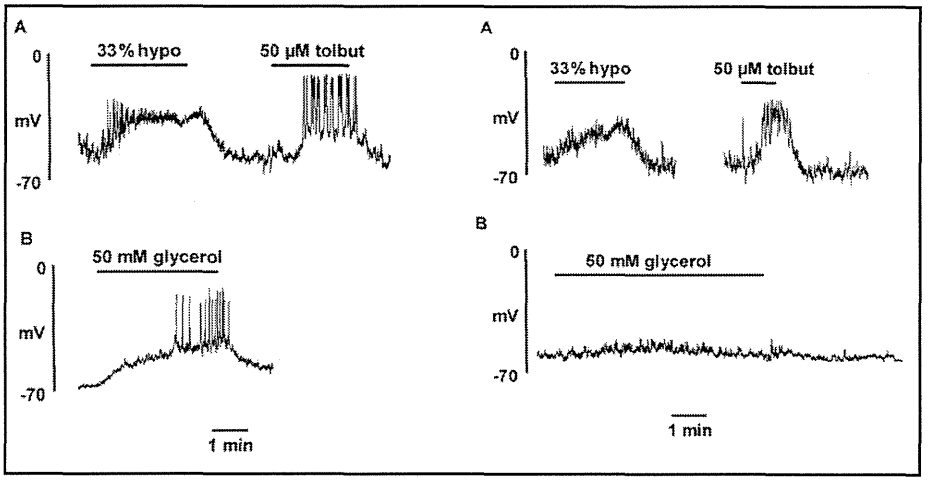

Fig. 8. Effects of either a 33% decrease in extracellular osmolarity or the administration of 50 µM tolbutaminde to cells exposed to 2.8 mM D-glucose (A) and the substitution of 50 mM mannitol by 50 mM glycerol in the presence of 2.8 mM D-glucose (B) on membrane potential in AQP7$^{+/+}$ (left panel) or AQP7$^{-/-}$ (right panel) mouse pancreatic β-cells. Recording are representative of 3 - 4 cells.

recorded in the same type of mice (control or knock-out mice) when the islets were eventually exposed to only 2.8 mM. Likewise, when the islets were eventually incubated at 16.7 mM D-glucose, the paired incubation/preincubation ratio for insulin output was lower ($p < 0.001$) in the knock-out mice (253.9 ± 48.4%; n = 23) than in the control mice (676.2 ± 89.8%; n = 16).

The unfavourable effect of the absence of AQP7 affected to the same relative extent the secretory response to distinct secretagogues. Indeed, the incubation/preincubation ratio for insulin release from the islets of knock-out mice averaged, in the first series of experiments, i.e. in islets eventually incubated at 2.8 mM D-glucose in media deprived of 50 mM NaCl, whether in the absence or presence of 100 mM glycerol, 51.7 ± 6.2% (n = 35) of the corresponding reference values found within the same experiments and under the same experimental conditions in the AQP7$^{+/+}$ mice (100.0 ± 12.2%; n = 40), the former value not being significantly different ($p > 0.45$) from that recorded in the second series of experiments, i.e. in islets eventually exposed to 8.3 or 16.7 mM D-glucose, in witch case the mean value found in the AQP7$^{-/-}$ mice averaged 46.3 ± 5.5% (n = 46) of the corresponding reference values (100.0 ± 9.8%; n = 31). In other terms, the relative magnitude of the decrease in the secretory response of islets from AQP7$^{-/-}$ mice was virtually identical ($p > 0.75$) in the first (48.3 ± 14.2%; df = 73) and second (53.6 ± 10.5%; df = 75) set of experiments.

Cell volume changes in response to extracellular hypotonicity, D-glucose or glycerol

Fig. 5A shows volume changes in mouse β-cells superfused with hypotonic solutions. When exposed to